sustainability

Article

DEM Study on Hydrological Response in Makkah City, Saudi Arabia

Asep Hidayatulloh [1], Anis Chaabani [1], Lifu Zhang [2] and Mohamed Elhag [1,2,3,4,*]

[1] Department of Hydrology and Water Resources Management, Faculty of Meteorology, Environment & Arid Land Agriculture, King Abdulaziz University, Jeddah 21589, Saudi Arabia
[2] The State Key Laboratory of Remote Sensing, Aerospace Information Institute, Chinese Academy of Sciences, Beijing 100101, China
[3] Department of Geoinformation in Environmental Management, CI-HEAM/Mediterranean Agronomic Institute of Chania, 73100 Chania, Greece
[4] Department of Applied Geosciences, Faculty of Science, German University of Technology in Oman, Muscat 1816, Oman
* Correspondence: melhag@kau.edu.sa

Abstract: The changes in catchments can be analyzed through the generation of DEM, which is important as input data in hydrologic modeling. This study aims to analyze the effect of anthropogenic activities on hydrological studies based on DEM comparison and GIUH hydrographs. The four DEM datasets (SRTM, ALOS, Copernicus, Sentinel-1) were compared to the topographic map of Makkah City and GPS data in order to assess the quality of the DEM elevation. The GIS Arc Hydro toolbox was used to extract morphometric and Horton–Strahler ratio characteristics to generate a GIUH hydrograph of the catchments of Wadi Nouman and Wadi Ibrahim inside Makkah City. Based on the DEM comparison, Copernicus and SRTM have the highest accuracy, with R^2 = 0.9788 and 0.9765, and the lowest RMSE, 3.89 m and 4.23 m, respectively. ALOS and Sentinel-1 have the lowest R^2, 0.9687 and 0.9028, and the highest RMSE, 4.27 m and 6.31 m, respectively. GIUH Copernicus DEM on Wadi Nouman has a higher q_p and lower t_p (0.21 1/h and 2.66 h) than SRTM (0.20 1/h and 2.75 h), respectively. On Wadi Ibrahim, the SRTM has a greater q_p and lower t_p than Copernicus due to the wadi having two shapes. Based on the anthropogenic effect, the stream network in the mountain area is quite similar for SRTM and Copernicus due to the dominant influence of the mountainous relief and relatively inconsequential influence of anthropogenic activities and DEM noise. In the urban area, the variation of the stream network is high due to differing DEM noise and significant anthropogenic activities such as urban redevelopment. The Copernicus DEM has the best performance of the others, with high accuracy, less RMSE, and stream flow direction following the recent condition.

Keywords: DEM; anthropogenic activities; hydrological study; Sentinel-1; Makkah City

check for updates

Citation: Hidayatulloh, A.; Chaabani, A.; Zhang, L.; Elhag, M. DEM Study on Hydrological Response in Makkah City, Saudi Arabia. *Sustainability* **2022**, *14*, 13369. https://doi.org/10.3390/su142013369

Academic Editor: Andrzej Walega

Received: 18 July 2022
Accepted: 9 October 2022
Published: 17 October 2022

Publisher's Note: MDPI stays neutral with regard to jurisdictional claims in published maps and institutional affiliations.

Copyright: © 2022 by the authors. Licensee MDPI, Basel, Switzerland. This article is an open access article distributed under the terms and conditions of the Creative Commons Attribution (CC BY) license (https://creativecommons.org/licenses/by/4.0/).

1. Introduction

The water resource system and hydrological condition of a catchment can be influenced by human activities or anthropogenic activities and climate change. Climate change refers to meteorological factors, such as extreme precipitation and rising temperature, causing changes in the water cycle of catchments and flash floods as a natural common disaster. In the hydrological field, it also changes the character of the catchment, such as the stream flow of the catchment and its morphometric parameters [1,2]. Wang et al. [3] carried out hydrological modeling in three river basins—Chaohe, Zhanghe, and Hutuo River—which found that anthropogenic activities are the dominant factor in stream flow changes rather than climate change. Tang et al. [4] found human activities in the Lancang River basin in China have a 55–60% contribution greater than climate change, with 42.6% on average. There are several studies regarding hydrological responses due to anthropogenic activities, such as groundwater contaminants on the Tarsus coastal plain, Turkey [5], catchment health in the Shazand catchment, Iran [6], and stream flow and geomorphological changes of catchments [7–10]. Hydrological alterations to Krishna River, India [11], were studied as an effect of dam constructions (pre and post constructions), and the hydrological alteration or flow changes were measured. All the previous studies proved that anthropogenic activities significantly affect the hydrological field, ecosystem, and river system [12,13].

The study of catchment changes can be done through the Digital Elevation Model (DEM) using the remote sensing (RS) technique. The DEM data represent the elevation or topography of the earth's surface, which is very important for environmental studies [14], such as catchment delineation [15,16], stream network extraction [17,18], surface flow path mapping [19], different types of natural hazards [20], and also to model floods [21,22]. Various global open DEMs, such as Shuttle Radar Topography Mission (SRTM) from NASA, Advanced Land Observing Satellite (ALOS) from JAXA, and Copernicus from ESA, can be accessed freely online. In Addition, the DEM data derived from two Sentinel-1 images can be an alternative using the InSAR technique. Numerous DEM comparison studies have been carried out by researchers to select the proper DEM for applications. Purinton and Bookhagenm [23] compared SRTM-NASADEM, ASTER-GDEMv3, ALOS-W3Dv3.1, TanDEM-X, and Copernicus and found that the Copernicus DEM has the most realistic height representation, with low pixel-to-pixel noise and no longer wavelength artifacts, located in the arid and steep area in Argentina. Karlson et al. [24] compared four pan-Arctic DEMs within the Kalix River catchment in northern Sweden and found Copernicus produced the most accurate elevation, small mean error, and RMSE, and was most similar to the reference DEM, followed by Arctic DEM and ALOS, the least accurate being ASTER. Karki et al. [25] compared river basins in Nepal and found SRTM 90 m more suitable for the large river basin and HydroSHEDS preferable for a small–medium basin, while CARTO and ASTER were far behind in accuracy compared to the other DEMs across all basins.

The study of catchment changes and their behavior can also be analyzed through morphometric parameters based on the physiographic features of the catchment [26,27]. The morphometric studies of a catchment can be investigated based on the determination of the geomorphological unit hydrograph (GIUH). Rodríguez-Iturbe and Valdés [28] stated that GIUH is a hydrograph that depends on the morphological parameters of the catchment. The DEM is the main data used for the extraction of the stream network by defining the stream threshold area. The Horton–Strahler ratios, i.e., bifurcation ratio, length ratio, and area ratio, and the mainstream length from morphometric parameters, can be used for generating the GIUH [29]. Based on this study, the comparison of past and recent conditions can be evaluated.

This study aims to analyze the effect of anthropogenic activities on the hydrological study in Makkah City based on a comparison of DEM datasets. The variation of morphometric parameters, the stream network, and Horton ratios from various DEM were analyzed to measure the parameters q_p and t_p of the GIUH. This study is useful for hydrologists and policymakers for catchment management purposes.

2. Study Area

Makkah City is the administrative capital of the Makkah Region, with an area of around 1.200 km^2 and an elevation of 277 m AMSL, 80 km inland from the Red Sea. It lies between 39°53′ E to 40°02′ E and 21°09 N to 21°37′ N. The urbanization rate in Makkah City is very high. Based on the census of 2017, the population in Makkah City is around 2,017,793, with an area covered by 33,354 ha. This is almost twice that of 2003, when the population was 1,375,000 and the city had an area of 20,800 ha, with a population density of 60.49 p/ha. (The Ministry of Municipal and Rural Affairs, https://www.my.gov.sa/wps/portal/snp/main, accessed on 17 July 2022).

The topography conditions in Makkah City are quite complex based on the surrounding mountains along the residential area in the city, especially near Haram Mosque. Geologically, Makkah City contains three types of rock: igneous, metamorphic, and sedimentary. In the mountains of Makkah, Precambrian rock is dominant, with schist, amphibolites, and gneiss. The surface of Makkah City is also crossed by several structural valleys, faults, and cracks [30,31]. The Wadi Ibrahim catchment, especially, contains Precambrian rock such as quartz diorite and tonalite as the main igneous rock [32].

There are some wadies or catchments in the Makkah City area: Wadi Nouman, Wadi Al-Sharea, Wadi Urainah, Wadi Muhassar, Wadi Ibrahim, and Wadi Al-Selouly (Figure 1).

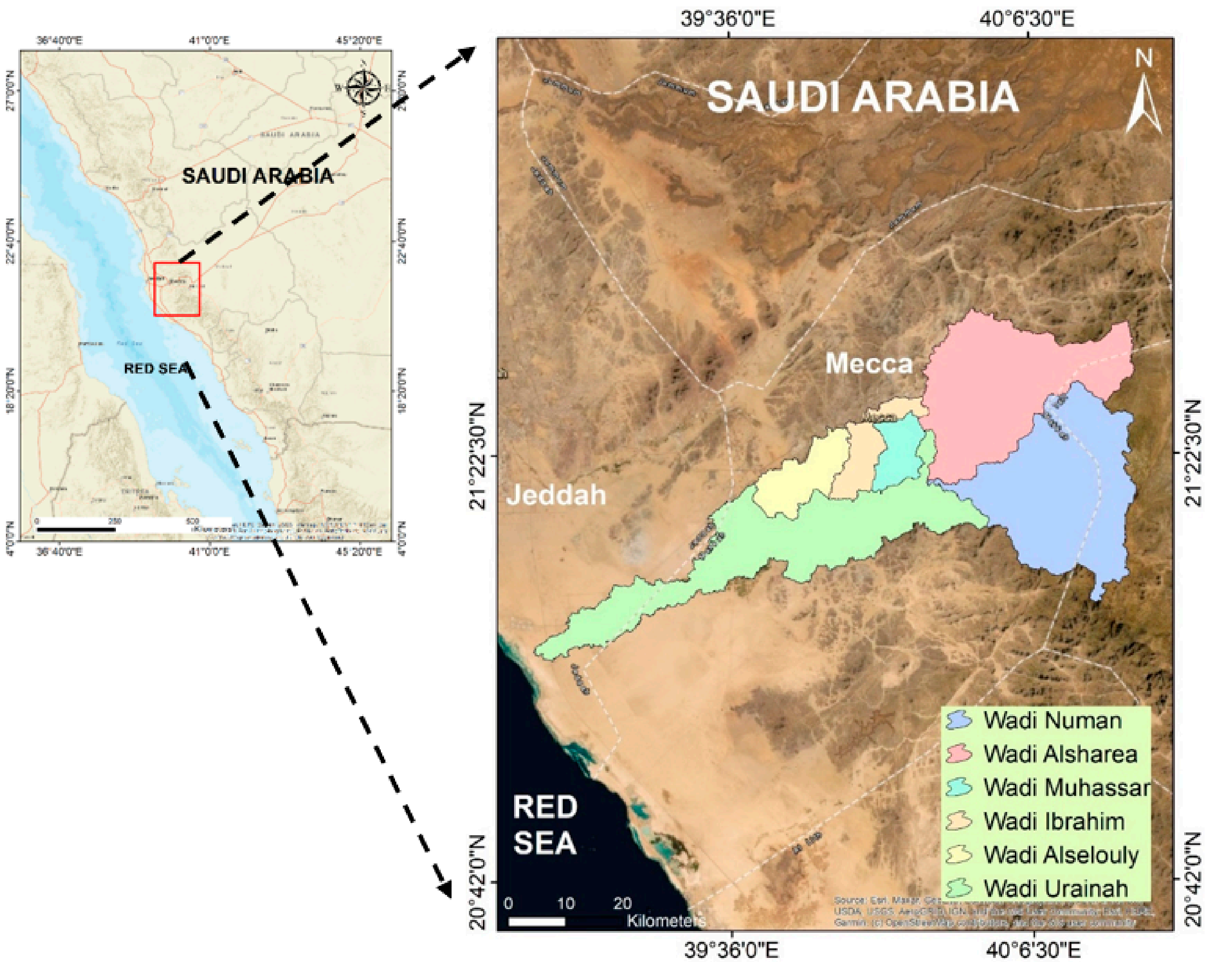

Figure 1. Several wadi and catchments in Makkah City, Saudi Arabia (Source arcSource: Esri, Maxar, GeoEye, Earthstar Geographics, CNES/Airbus DS, USDA, USGS, AeroGRID, IGN, and the GIS User Community).

Wadi Ibrahim catchment is one of the most important in Makkah City due to the Al-Haram Mosque located in the lower part of Wadi Ibrahim, and the well of Zamzam around 20 m east of Kaaba and about 30 m deep. Catchments in Makkah City are categorized as arid catchments characterized by less precipitation, drought, and scarcity of water resources. The annual rainfall of Makkah City varies, recorded since 1966 after the installation of gauge station in situ instruments at Umm Al-Gud, Makkah, by the Saudi Meteorological Authority, and in 1989 at Umm al-Qura University. In 1966, the annual rainfall was less than 5 mm, while 1989 had an annual rainfall of 318 mm. The extreme rainfall in 1989 saw 269 mm in a single storm, causing flash flood hazards and the runoff to enter the Al-Haram Mosque area, with Kaaba being half-inundated [33].

3. Material and Methodology

3.1. Open Global DEM

Various global open DEMs were used in this study, such as the Shuttle Radar Topography Mission (SRTM) from NASA, Advanced Land Observing Satellite (ALOS) from JAXA, and Copernicus from the European Space Agency (ESA). All of them are fully open access and can be downloaded freely through their websites (Table 1). In addition, the Sentinel-1 DEM can be retrieved from two Sentinel-1 images using the InSAR technique.

- SRTM

SRTM is DEM data provided by NASA with a research effort that obtained digital elevation models on a near-global scale. During the acquisition period in February 2000, the first version of SRTM was released in 2003 with three arc second, or approximately 90 m, resolution, and the new version has a resolution of one arc second (30 m), released in 2014. These DEM data can be obtained from https://earthexplorer.usgs.gov/, accessed on 25 October 2021.

- ALOS PALSAR

ALOS PALSAR using L-Band SAR, provided by JAXA with an acquisition period from 2006 to 2011, contributes to the fields of mapping, disaster monitoring, precise regional land coverage observation, and resource surveying. The release year was 2014. The DEM can be downloaded from: https://search.asf.alaska.edu, accessed on 26 October 2021.

- Copernicus

The Copernicus DEM GLO-30-DTED is provided by ESA, an improvement product of commercial version TanDEM-X which was released in 2019 for 90 m and 2021 for 30 m. The acquisition period was 2011–2014. The Copernicus DEM data are available at three available spatial resolutions (10 m, 30 m, and 90 m). Unfortunately, the 10 m resolution is available only for the Europe area. The source of the Copernicus DEM is https://panda.copernicus.eu/web/cds-catalogue/panda, accessed on 27 October 2021.

3.2. DEM Sentinel-1 Generation

DEM can be obtained from a pair of Sentinel-1 SLC images by creating an interferogram and unwrapping phase process [34]. An interferogram can be generated by combining the phase of two images with the co-registration process. The quality of the Sentinel-1 DEM depends on the quality of images during pair image selection, the criteria of which are as follows:

- Perpendicular baseline: The perpendicular baseline (the position of the satellite at the time of acquisition) of the image should have a range of 150–300 m (ESA). The perpendicular baseline is the distance between the satellite's position at the time of image acquisition. This is different to displacement studies that required a small baseline; DEM generation required a high baseline.
- Temporal baseline: The temporal baseline (different time acquisition) of the image should be as short as possible (6–12 days) to reduce the risk of temporal decorrelation of the phase. The short temporal baseline gives the best result, while the long temporal baseline led to a bad interferogram.
- Atmospheric condition: Some factors in the atmosphere, such as water vapor, can reduce the coherence and quality of the results because they cause phase delays. The recommended condition is good weather and dry conditions with no rainfall.
- Both images must have the same direction: ascending or descending

Figure 2 shows the pair image selection process in the ASF's (Alaska Satellite Facility) baseline tools. The information of 16 chosen images from Sentinel-1 is shown in Table 1.

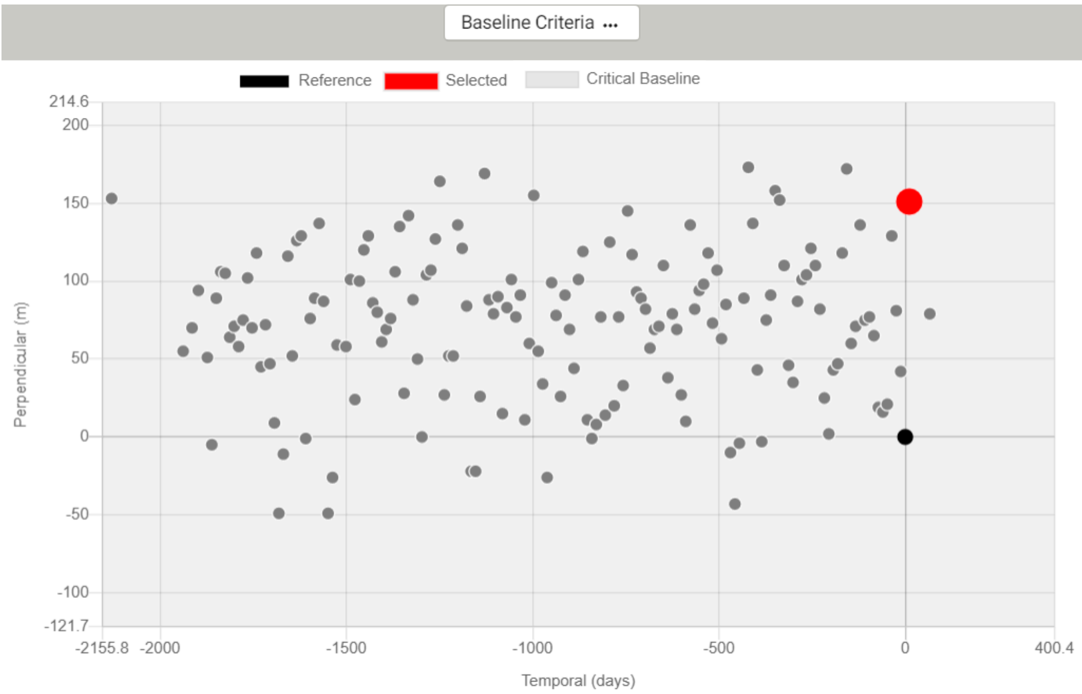

Figure 2. Image baseline selection on the ASF website.

Table 1. Detail information of two Sentinel-1 images (master and slave).

Type	Date	Track	Orbit	b_temp (days)	b_perp (m)	Coherence
Master	02-September-2017	14	7215	0	0	1
Slave	14-September-2017	14	7390	12	136	0.88
Master	28-August-2018	14	12,465	0	0	1
Slave	15-October-2018	14	13,165	48	158	0.83
Master	21-September-2018	14	12,815	0	0	1
Slave	15-October-2018	14	13,165	24	107	0.89
Master	15-October-2018	14	13,165	0	0	1
Slave	08-November-2018	14	13,515	24	191	0.82
Master	27-October-2018	14	13,340	0	0	1
Slave	08-November-2018	14	13,515	12	143	0.87
Master	22-September-2020	14	23,490	0	0	1
Slave	16-October-2020	14	23,840	24	175	0.83
Master	04-October-2020	14	23,665	0	0	1
Slave	16-October-2020	14	23,840	12	84	0.92
Master	21-November-2020	14	24,365	0	0	1
Slave	08-January-2021	14	25,065	48	151	0.84
Master	10-December-2021	14	30,140	0	0	1
Slave	22-December-2021	14	29,965	12	153	0.86

b_temp is the temporal baseline, b_perp is the perpendicular baseline, and coherence is a value that expressed the similarity of the radar reflection between two SAR images.

Few techniques are used to retrieve Sentinel-1 DEM, such as TOPSAR Split to select the area of interest. The orbit file operator corrects the orbit error. In this study, Sentinel precise (auto download) was chosen rather than Sentinel restituted for orbit determination.

The Sentinel precise orbit has less than 5 cm accuracy and the files are delivered within 20 days after data acquisition, while Sentinel restituted has a 10 cm accuracy, with files delivered three days after data acquisition. In this study, the DEM product was created manually from Sentinel-1 compared with four different open global DEM products, such as SRTM, ALOS, and Copernicus (Table 2). The flowchart for generating Sentinel-1 DEM is shown in Figure 3 and is described in Table 3.

Table 2. General information on various DEM characteristics.

DEM	Parameter				
	Resolution	Sources	Acquisition Year	Released Year	Band
SRTM	30 m	NASA	2000	2013	C
ALOS	12.5 m	JAXA	2009	2014	L
Copernicus	30 m	ESA	2011–2014	2021	X
Sentinel-1	13.5 m	ESA	2015–Now	2015	C

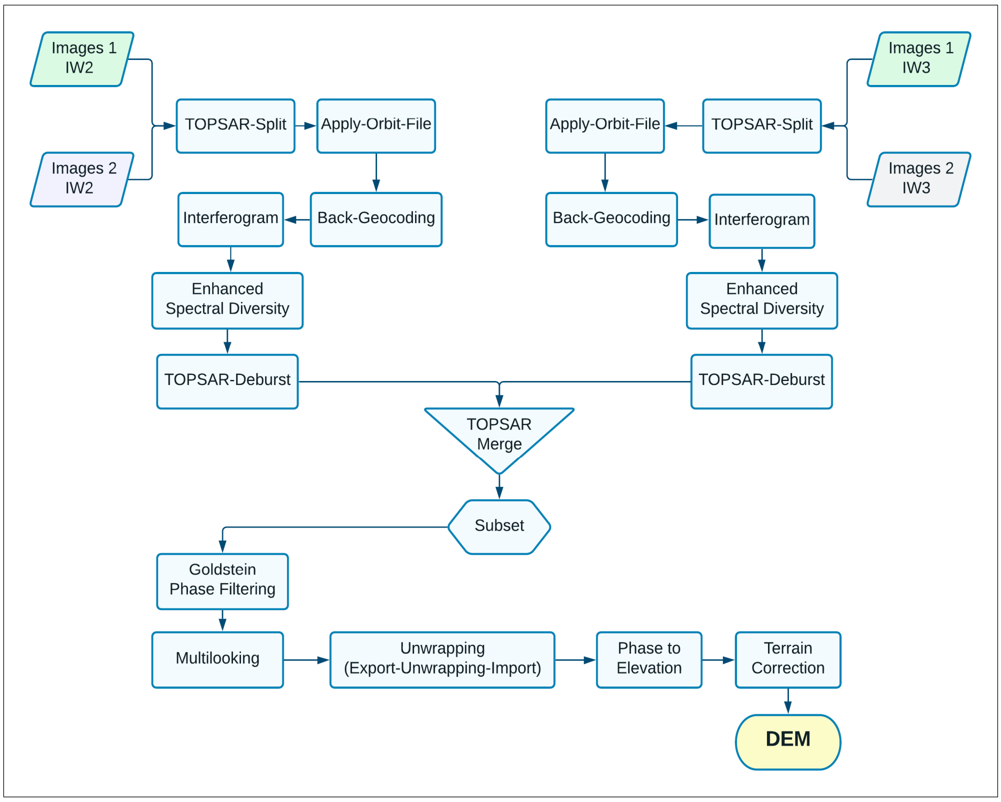

Figure 3. Flowchart of DEM generation based on the Sentinel-1 images using SNAP software.

Table 3. The description of each step of DEM generation is sketched in Figure 3.

Steps	Descriptions
Read data	Read data from two different SAR images
TOPSAR Split	Select the area of interest (IW2 and IW3, bursts 2–5, VV Polarization)
Apply Orbit File	Correct satellite and orbit geometry
Back Geocoding	Make over stack between two images
Interferogram	Generate phase and coherence
TOPSAR deburst	Remove the seamline/space between the bursts
TOPSAR merge	Merge the subswath IW2 and IW3
Goldstein Phase Filtering	Reduce the phase noise
Multilooking	Reduce the inherent speckle noise
Snaphu unwrapping	Export, unwrapping, and import of phase
Phase to Elevation	Convert phase to elevation (DEM)
Terrain Correction	Geometric correction to project the map into WGS84

3.3. GIUH Estimation

The GIUH estimation flowchart is shown in Figure 4 and described for each step as follows:

1. Fill sinks and compute the flow direction and flow accumulations of the DEM using the eight-direction method.
2. Obtain stream network by applying a threshold area of 2 km^2 of the flow accumulation.
3. Delineate the catchment and extract its morphometric parameters using Arc Hydro tools and the morphometric toolbox in GIS.
4. Calculate Horton ratio parameters (R_B, R_L, R_A, L_Ω) and stream order w through the Python program "CalMorph" [35,36].

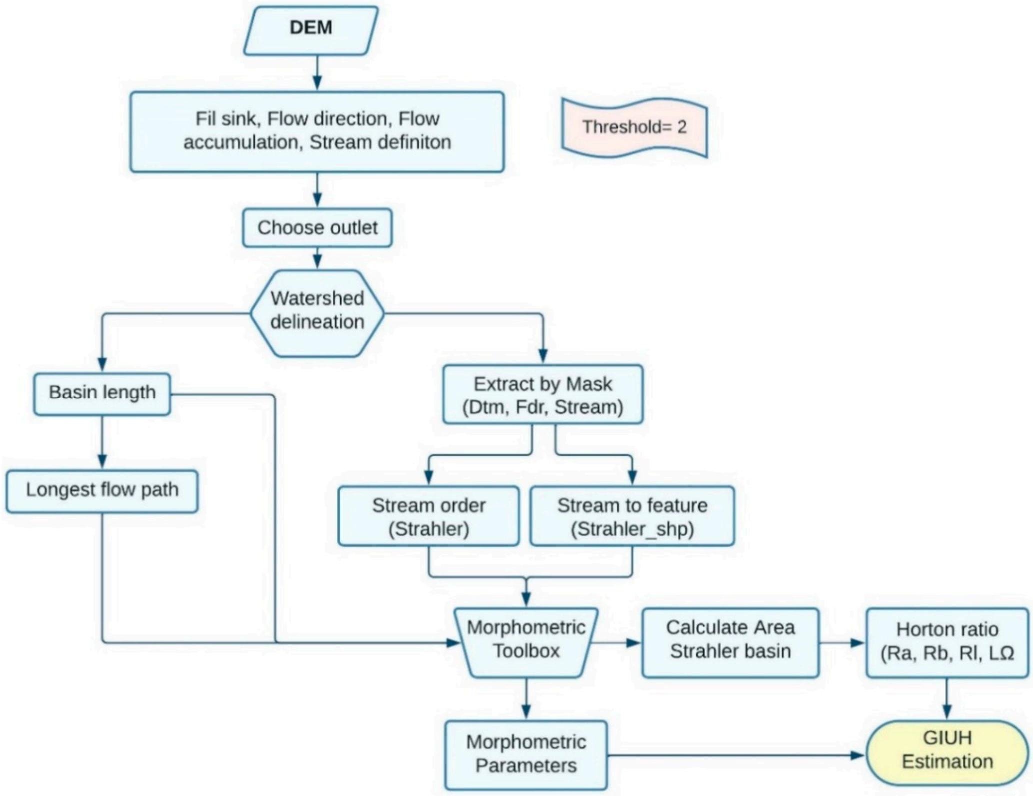

Figure 4. Flowchart of morphometric parameter extraction and GIUH estimation.

3.4. Horton Ratios

Horton–Strahler ratios proposed by Horton [37] include bifurcation ratios (R_B), length ratios (R_L), and area ratios (R_A), which have an expression as follows:

$$R_B = \frac{N(w)}{N\ (w+1)} \tag{1}$$

$$R_L = \frac{L(w+1)}{L(w)} \tag{2}$$

$$R_A = \frac{A(w+1)}{A(w)} \tag{3}$$

where $N(w)$ and $N(w+1)$ is the number of stream order w and for the next order, $L(w)$ and $L(w+1)$ are the mean length of stream order w and for the next order, and $A(w)$ and $A(w+1)$ are the mean area contributing to stream order w and for the next order $(w+1)$.

3.5. Nash Model

Nash (1960) [38] proposed the equation for GIUH estimation based on Horton ratios as shown below:

$$u(t) = \left(\frac{t}{k}\right)^{a-1} \frac{e^{-\frac{t}{k}}}{k\Gamma(a)} \tag{4}$$

where:
$u(t)$ = GIUH parameter
t = Time (hours)
$\Gamma(a)$ = Gamma function
k = Shape and scale parameters proposed by Rosso [39]:

$$a = 3.29\left(\frac{R_B}{R_A}\right)^{0.78} {R_L}^{0.07} \tag{5}$$

$$k = 0.70\left(\frac{R_A}{R_B R_L}\right)^{0.48} \frac{L_\Omega}{v} \tag{6}$$

where L_Ω is the length of the highest order stream and v is the velocity of the flow

$$v = 0.8562\ L^{0.23} {S_B}^{0.385} \tag{7}$$

where L is the length of the stream and S_B is the mean slope of the catchment. The peak discharge (q_p) and time to peak (t_p) of the GIUH are given by Rodríguez-Iturbe and Valdés [28]:

$$q_p = \left(\frac{1.31}{L_\Omega}\right) R_L^{0.43}\ v \tag{8}$$

$$t_p = 0.44\left(\frac{R_B}{R_A}\right)^{0.55} {R_L}^{-0.38} \frac{L_\Omega}{v} \tag{9}$$

The flowchart of morphometric parameters of catchment and GIUH estimation is shown in Figure 4.

3.6. DEM Validation

The elevation results from open access DEM data are not free from error and require validation of data accuracy. In this study, the reference elevation data was used from the topographical map of Makkah City, published by the Ministry of Petroleum and Mineral Resources Aerial Survey Department, KSA in 1975, and GPS data. The projection of the topographical map is Universal Transverse Mercator (UTM), with Ain Al Abd 1970 as the local datum, and has a scale of 1:50.000. The geo-referencing technique was used to import the scanned map into the ArcMap platform and to retrieve the elevation values from the 135 randomly distributed samples. Overall, there are 167 samples (Z value) consisting of 32 field measurement points collected by GPS around areas affected by the demolition of hills and near the mega project of the holy mosque expansion, and 135 points extracted from the topographical map. These samples are compared to the four DEM datasets in order to assess the quality of the data (Figure 5). Extra multi-value-to-point tools in GIS are used to combine the DEM and topographic map elevations. To assess the accuracy of each DEM dataset, statistical equation techniques are applied to different elevation datasets, mean absolute error (MAE), and Root Mean Square Error (RMSE), which are expressed as below:

$$Z_{error} = Z_{Topho} - Z_{DEM} \tag{10}$$

$$MAE = \sum_{i=1}^{n} \frac{|Z_{error}|}{n} \tag{11}$$

$$RMSE = \sqrt{\frac{\sum_{i=1}^{n} (Z_{error})^2}{n}} \tag{12}$$

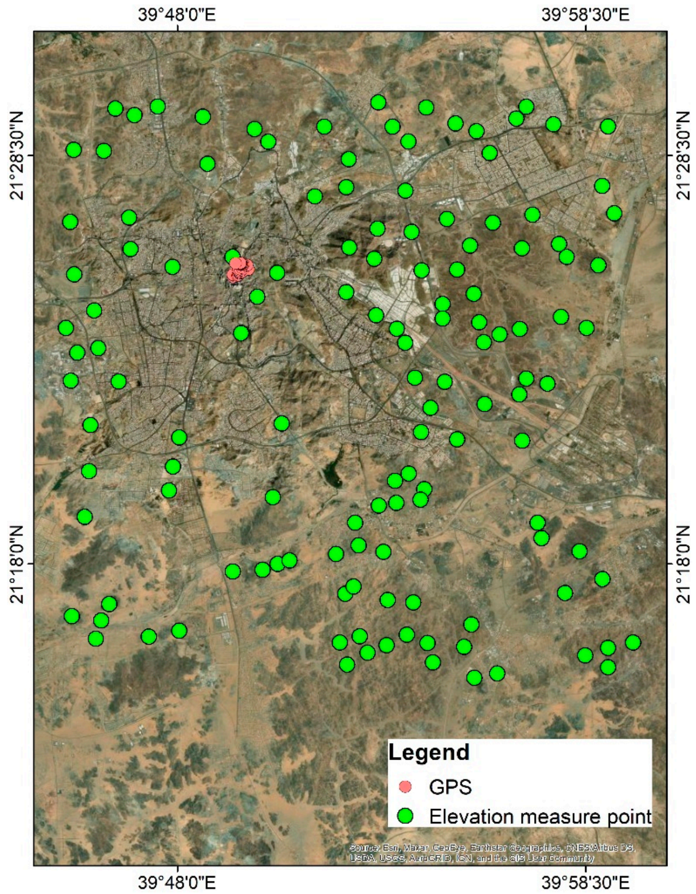

Figure 5. 167 random points selected for DEM comparison (Source arcSource: Esri, Maxar, GeoEye, Earthstar Geographics, CNES/Airbus DS, USDA, USGS, AeroGRID, IGN, and the GIS User Community).

The statistical measurements above were applied to 167 random points selected for an estimate of the elevation error. The correlation between DEM and topography is also analyzed by the coefficient of determination (R^2), which is derived from the trend line of the scatterplot. The 0 value represents no correlation, and the 1 value represents a perfect correlation.

4. Results

4.1. DEM of Sentinel-1

Various coherence histograms from eight pairs of Sentinel-1 images are shown in Figure 6. This comparison shows the effect of the temporal and perpendicular baseline on the quality of the coherence, as mentioned in Section 3.2. The *X*-axis of the histogram represents the coherence value, which ranges from 0 to 1. The highest value expresses a good radar reflection of two SAR images. The *Y*-axis represents the number frequency in pixels. The first histogram (top-left), with a baseline of 191 m and 24 days, has the worst result for the pair images dated 15 October 2018 and 08 November 2018, and the best performance comes from the last histogram (bottom-right) images for the pair images dated 10 December and 22 December 2021. The temporal baseline is 12 days at 153 m, which is around 90% more coherence than 0.5 and has an exponential shape.

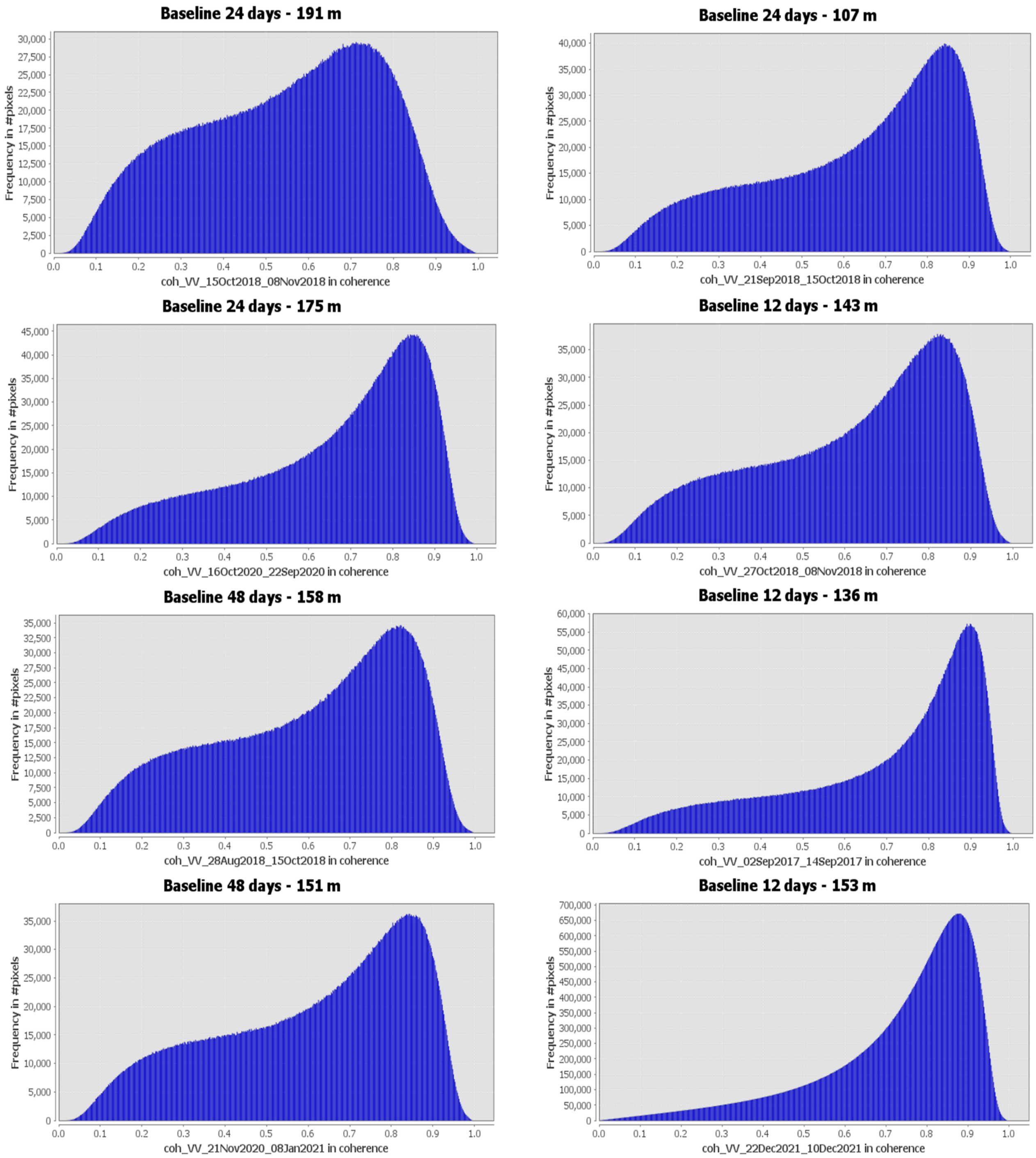

Figure 6. Coherence histogram of pairs of Sentinel-1 images.

Figure 7 shows DEM with hill shade of SRTM 30 m compared to the results of eight pairs of Sentinel-1 DEM images. The baseline at 12 days and 153 m on 10 and 22 December 2021 (top-middle) has the best result, which is close to the SRTM 30 m images. Based on the histogram coherence and hill shade results above, the pair of images on 10 December and 20 December 2021 were selected for DEM generation in this study.

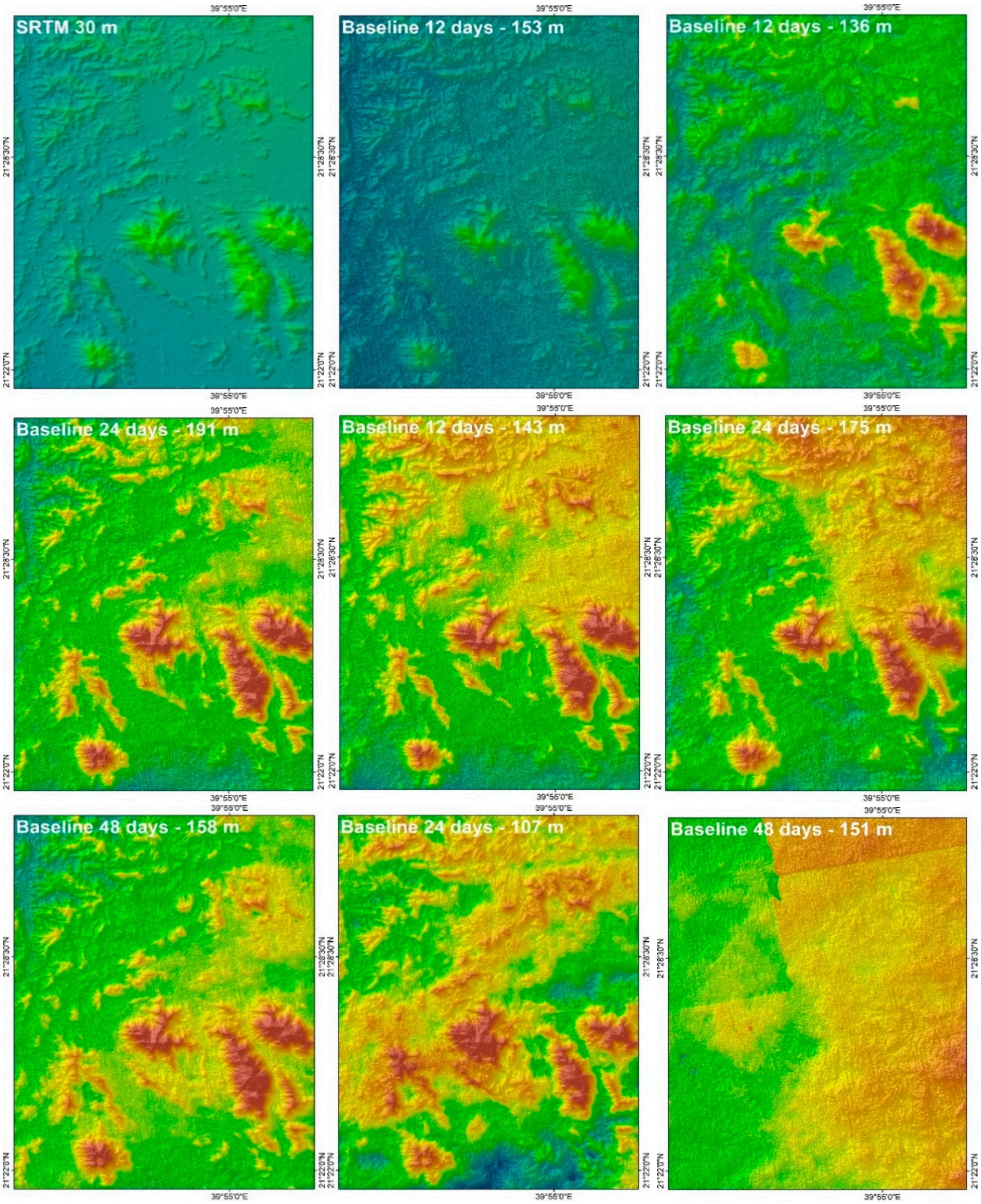

Figure 7. SRTM compared to eight DEM pairs from different temporal and perpendicular baselines in Sentinel-1 DEM.

4.2. DEM Comparison

The two catchments in Makkah City were delineated from four DEM datasets using the ArcHydro toolbox in GIS software. The wadies are the Wadi Nouman and Wadi Ibrahim catchments. Stream network extraction is carried out from the same threshold. The comparison of elevation and longest flow path of Wadi Nouman based on different DEM datasets is shown in Figure 8. Each DEM has a different shape due to different stream networks, and Sentinel is the most different to the others. The elevation of each DEM is also different due to each sensor having different interactions with surfaces. In Wadi Nouman, the low elevation from SRTM and Copernicus is 282 and 263 m, while Sentinel-1 has 504 m. The longest flow path for SRTM, ALOS, and Copernicus has an almost similar pattern, while Sentinel-1 has a quite different pattern and direction.

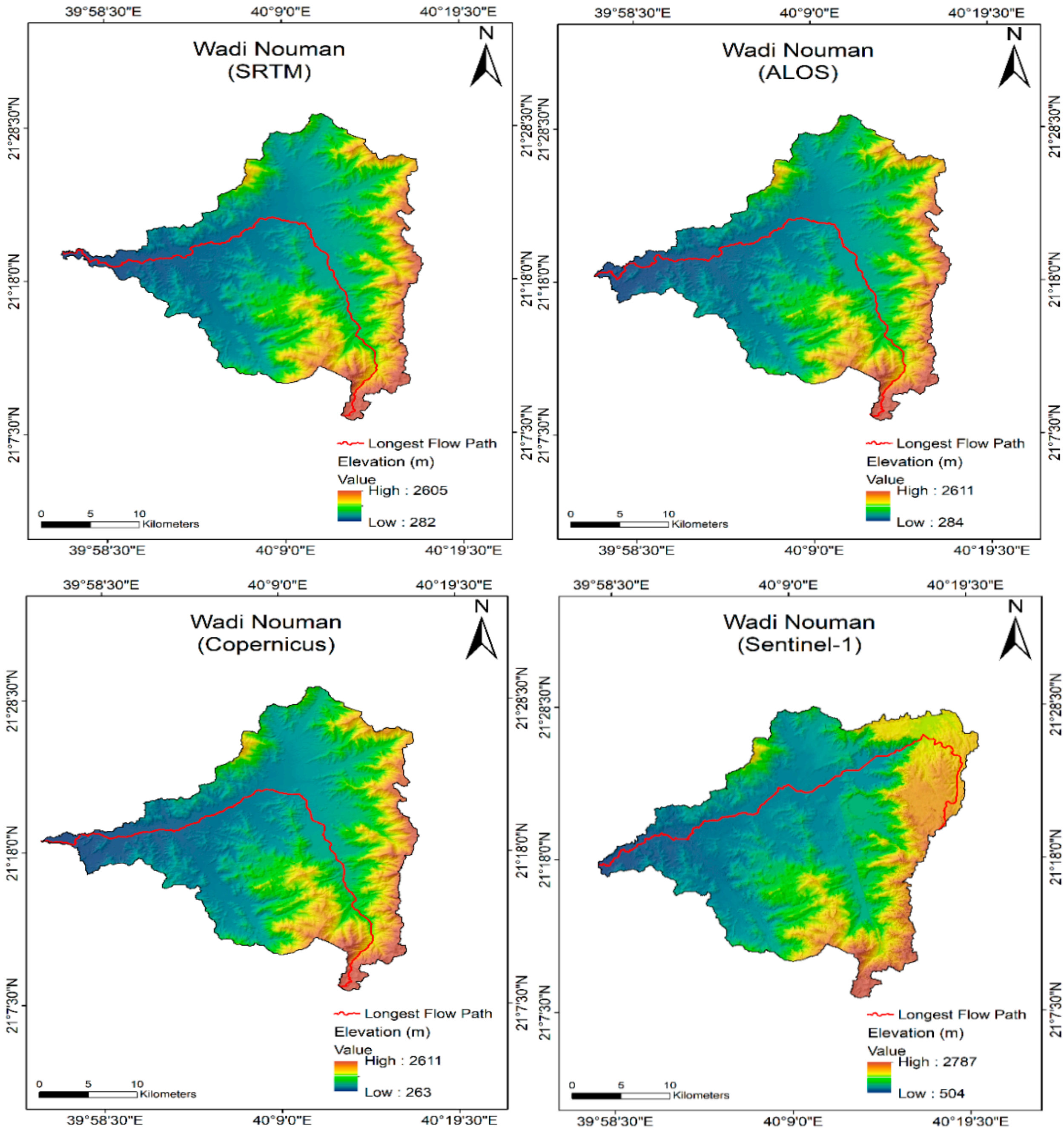

Figure 8. Elevation and longest flow path comparison of four DEMs of Wadi Nouman.

In Wadi Ibrahim, the wadi from Copernicus and Sentinel-1 has been divided into two sub-wadies. The low elevation from SRTM and ALOS is 213 m and 218 m, while that of Copernicus and Sentinel-1 is 199 m and 245 m, respectively. The shape of the wadi from Sentinel-1 and Copernicus is different due to changes in the stream network direction and location of the outlet. The elevation from Sentinel-1 is most significant for all wadies because of reasons such as poor coherence, baseline condition, atmospheric artifacts, and short wavelength (C-band). This factor can affect noise and error contribution (Figure 9).

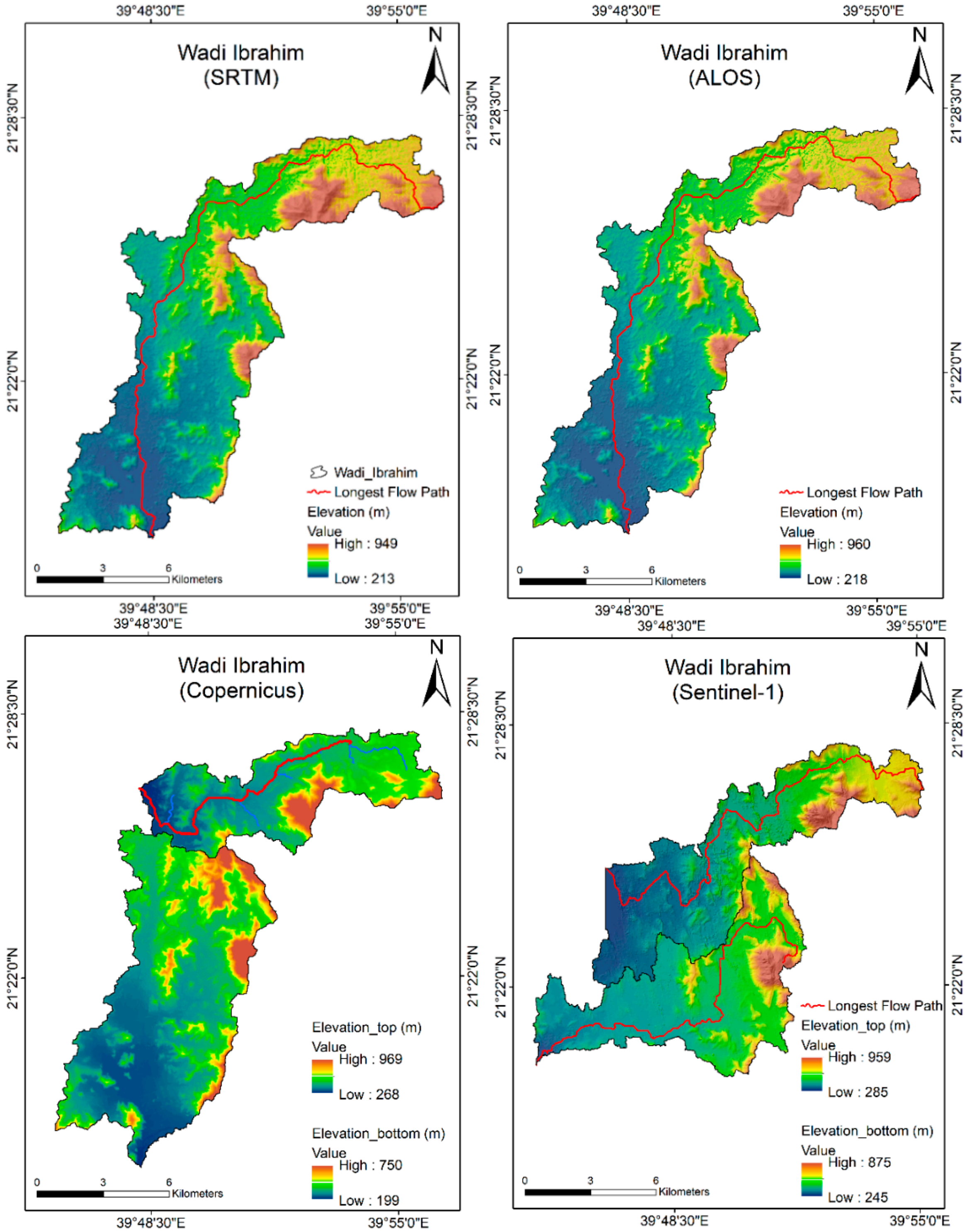

Figure 9. Elevation and longest flow path comparison of four DEMs of Wadi Ibrahim.

The catchment morphometric parameters of all DEMs have been obtained using ArcGIS software, shown in Table 4 for Wadi Nouman and Table 5 for Wadi Ibrahim.

Table 4. Morphometric parameters of Wadi Nouman catchment based on four DEMs.

Basin Parameters	Wadi Nouman			
	SRTM	ALOS	Copernicus	Sentinel-1
Low Elevation (m)	282	284	263	504
High Elevation (m)	2605	2611	2611	2787
Area (km)	678.6	695.7	694.9	747.7
Perimeter (km)	210.7	212.6	217.9	229.3
Longest flow path (km)	68.7	68.5	67.2	68.3
Basin Length (km)	47.4	47.2	49.3	41.2

Table 5. Morphometric parameters of Wadi Ibrahim catchment based on four DEMs.

Basin Parameters	Wadi Ibrahim					
	SRTM	ALOS	Copernicus (top)	Copernicus (bottom)	Sentinel (top)	Sentinel (bottom)
Low Elevation (m)	213	218	268	199	285	245
High Elevation (m)	949	960	969	750	959	875
Area (km)	110.8	110.3	41	79.6	56.5	53.1
Perimeter (km)	107.2	110.7	57	71.9	85.2	76.1
Longest flow path (km)	34.6	34.2	21.2	21.6	28.6	22.6
Basin Length (km)	28.6	28.8	15.8	16.4	18.7	14.9

Figures 10 and 11 show the comparison of the stream orders of two wadies for all DEM datasets. There are different numbers of stream orders. In Wadi Nouman (Figure 10), SRTM, Copernicus, and Sentinel-1 have four stream orders, while ALOS has five stream orders. Consequently, the L_Ω value of ALOS is different and unsuitable for comparison with the others. In Wadi Ibrahim, SRTM has the same shape as ALOS, but a different number of stream orders. The L_Ω of ALOS is higher than SRTM. In addition, Copernicus and Sentinel-1 have two wadies, but a different number of stream orders. It is difficult to compare them to each other.

Based on the procedures mentioned in Section 3.6, the statistical measurement result for four DEM datasets was calculated by comparing DEM to the topographic map of Makkah City. The scatter plot of 167 random points together with the trend line and its equations are shown in Figure 12. The Elevation error, MAE, and RMSE are calculated and presented in Table 6 to assess the accuracy of the DEM. Based on this calculation, Copernicus has the best performance with the smallest elevation error of 1963 m, RMSE of 3.89 m, and a correlation coefficient of 0.9788. The rank accuracy follows SRTM, ALOS, and Sentinel-1. SRTM has an elevation error of 2329 m, RMSE of 4.23 m, and a correlation coefficient of 0.9765. ALOS has a 2371 m elevation error with an RMSE of 4.27 m and a correlation coefficient of 0.9687. The worst results came from Sentinel-1 with an elevation error of 5174 m, RMSE of 6.31 m, and correlation coefficient of 0.9028, respectively. Sentinel-1 has the highest RMSE, which may be due to atmospheric noise contribution and an unsuitable temporal and perpendicular baseline.

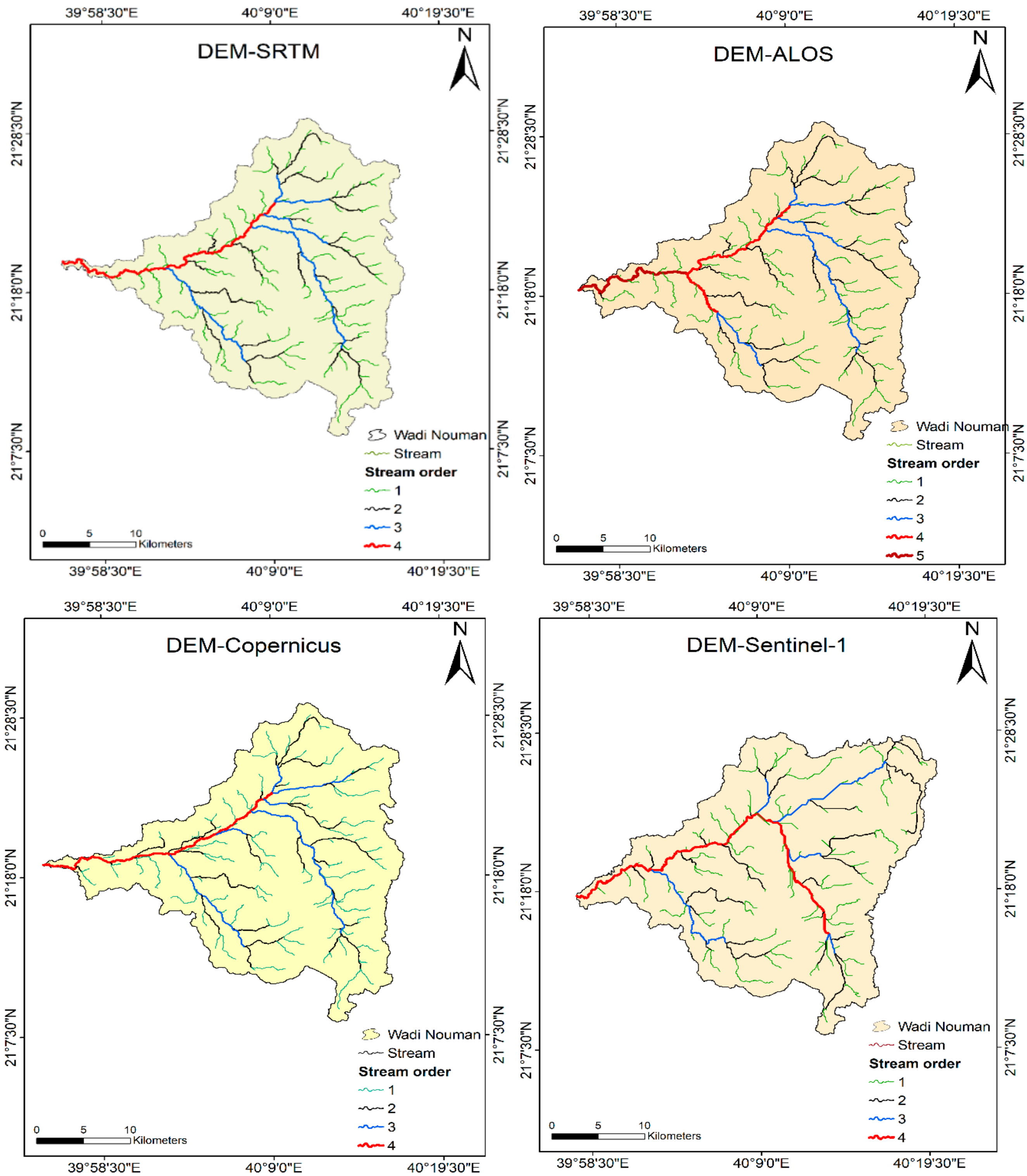

Figure 10. Comparison of stream order of Wadi Nouman, Makkah City.

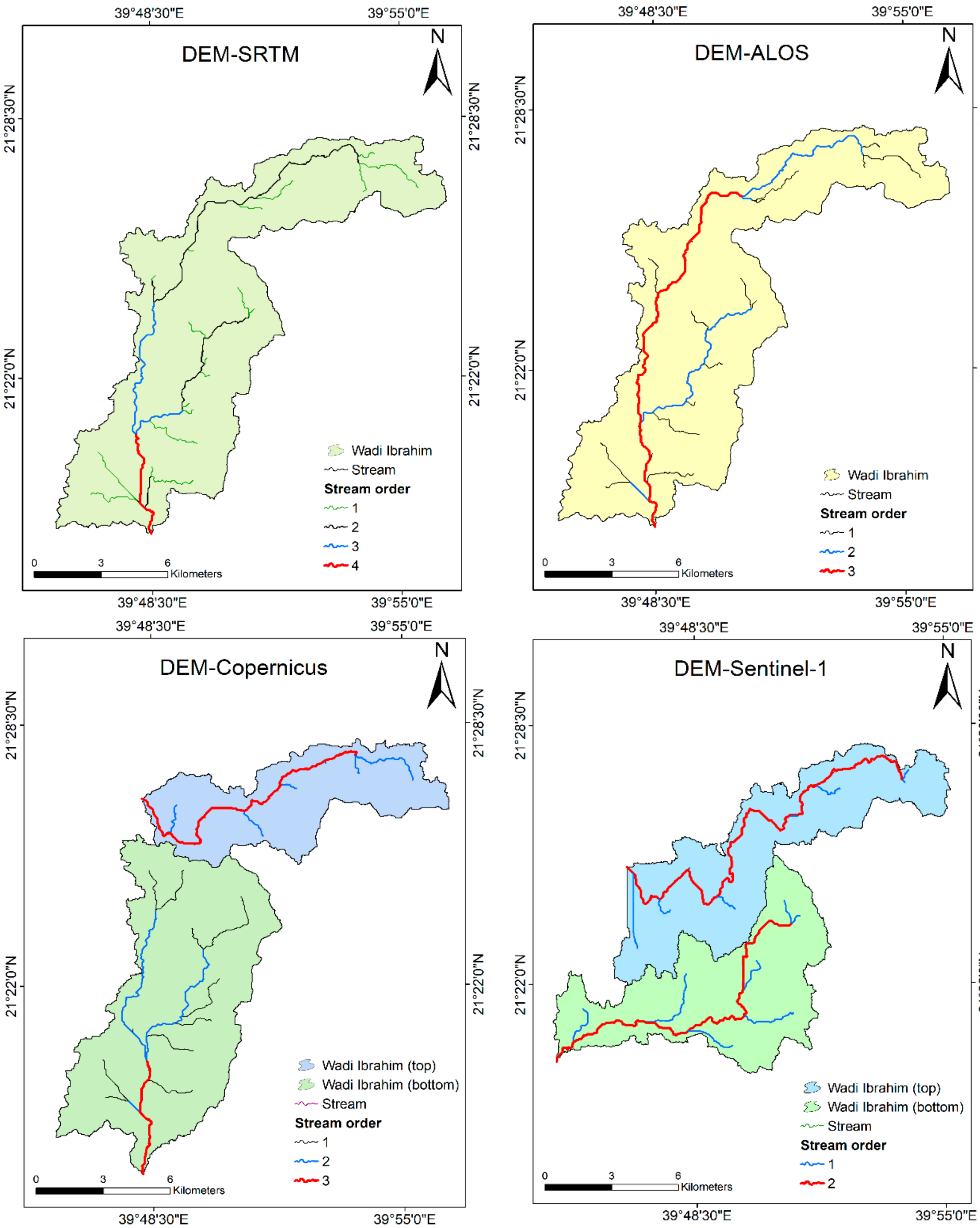

Figure 11. Comparison of stream order of Wadi Ibrahim, Makkah City.

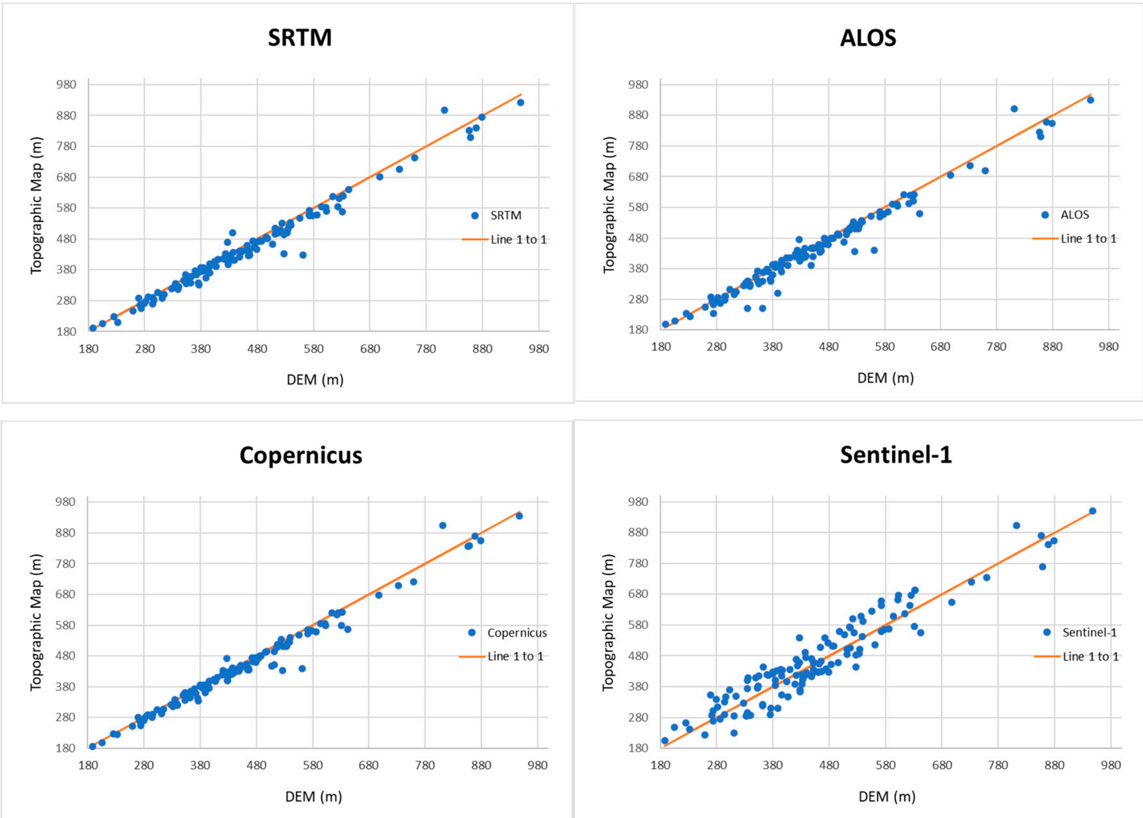

Figure 12. Scatterplot elevation comparison of topographic map vs. four DEM datasets.

Table 6. Statistical measurements of elevation error for each DEM dataset.

Statistical Parameters	DEM			
	SRTM	ALOS	Copernicus	Sentinel-1
Z_{Error} (m)	2329	2371	1963	5174
MAE (m)	17.92	18.24	15.1	39.8
RMSE (m)	4.23	4.27	3.89	6.31
R	0.9765	0.9687	0.9788	0.9028

Based on the DEM assessment and DEM comparison, the two highest errors were eliminated and were not processed for the next calculation on the hydrological process. The best two DEMs, SRTM and Copernicus, were then processed for hydrological assessment: SRTM as the old DEM (acquisition period in the year 2000) and Copernicus as the new DEM (acquisition period in the year 2011–2014). The Copernicus DEM has a new result for Wadi Ibrahim, which the stream network changes, and the basin is divided into two sub-basins. These results can be used to analyze five types of investigations: terrain surface changes caused by hill shade effects (Figure 13), topographical cross-section (Figure 14), historical imagery on Google Earth Pro (Figure 15), comparison on GIUH (Figures 16 and 17), and comparison of the mountainous and urban areas (Figure 18).

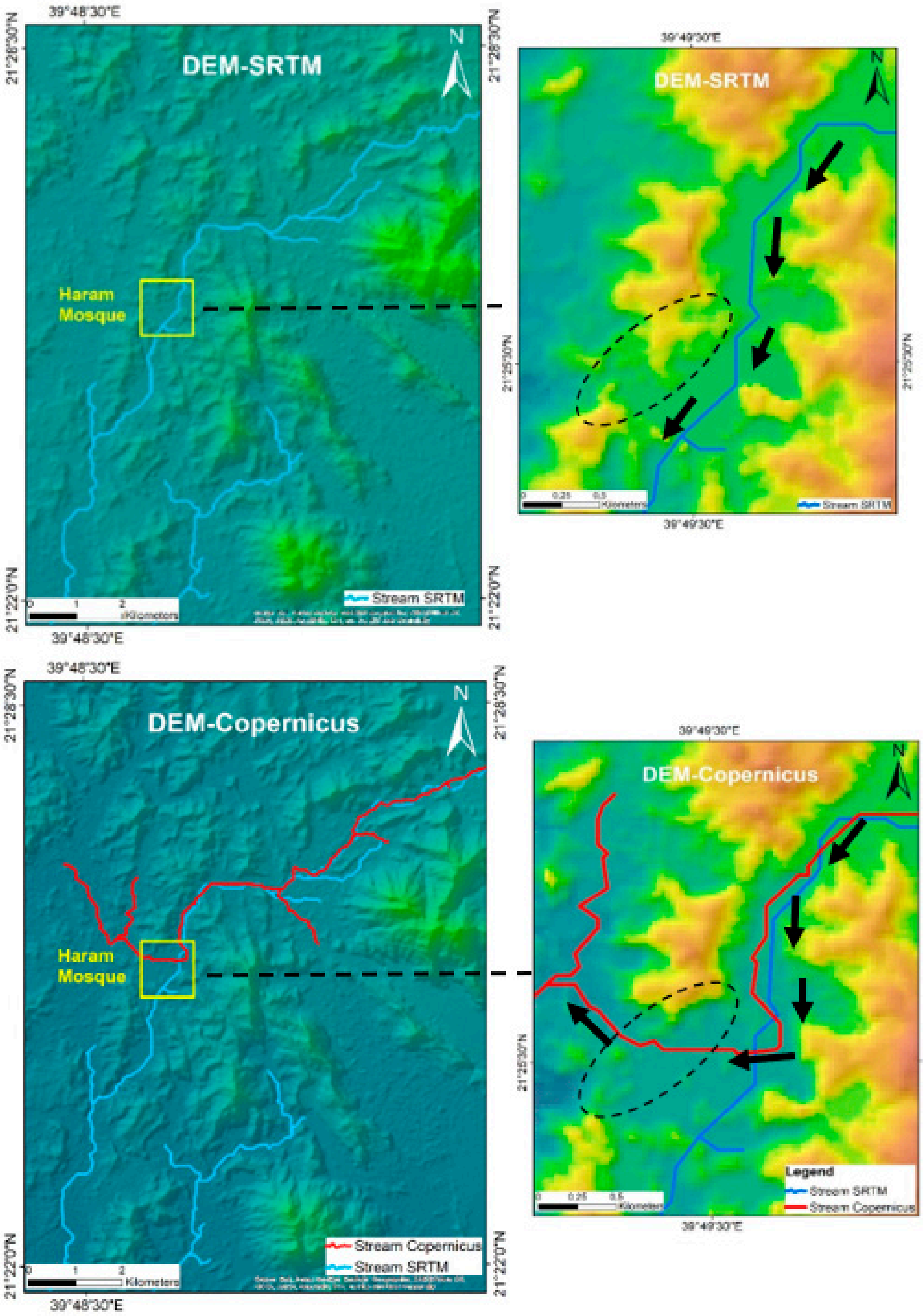

Figure 13. SRTM vs. Copernicus based on terrain surfaces (hillshade effect) (Source arcSource: Esri, Maxar, GeoEye, Earthstar Geographics, CNES/Airbus DS, USDA, USGS, AeroGRID, IGN, and the GIS User Community).

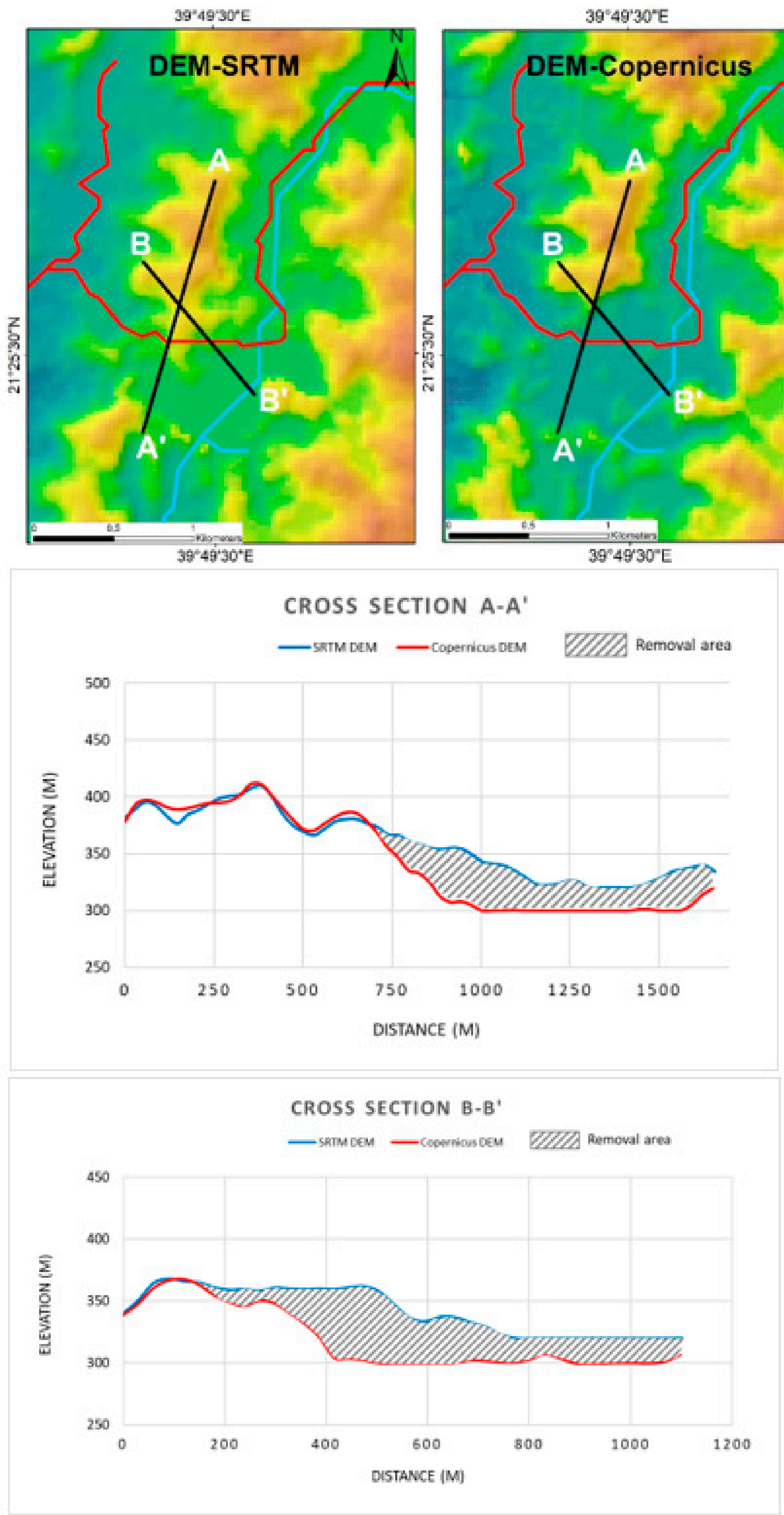

Figure 14. SRTM vs. Copernicus based on the topographical cross-section.

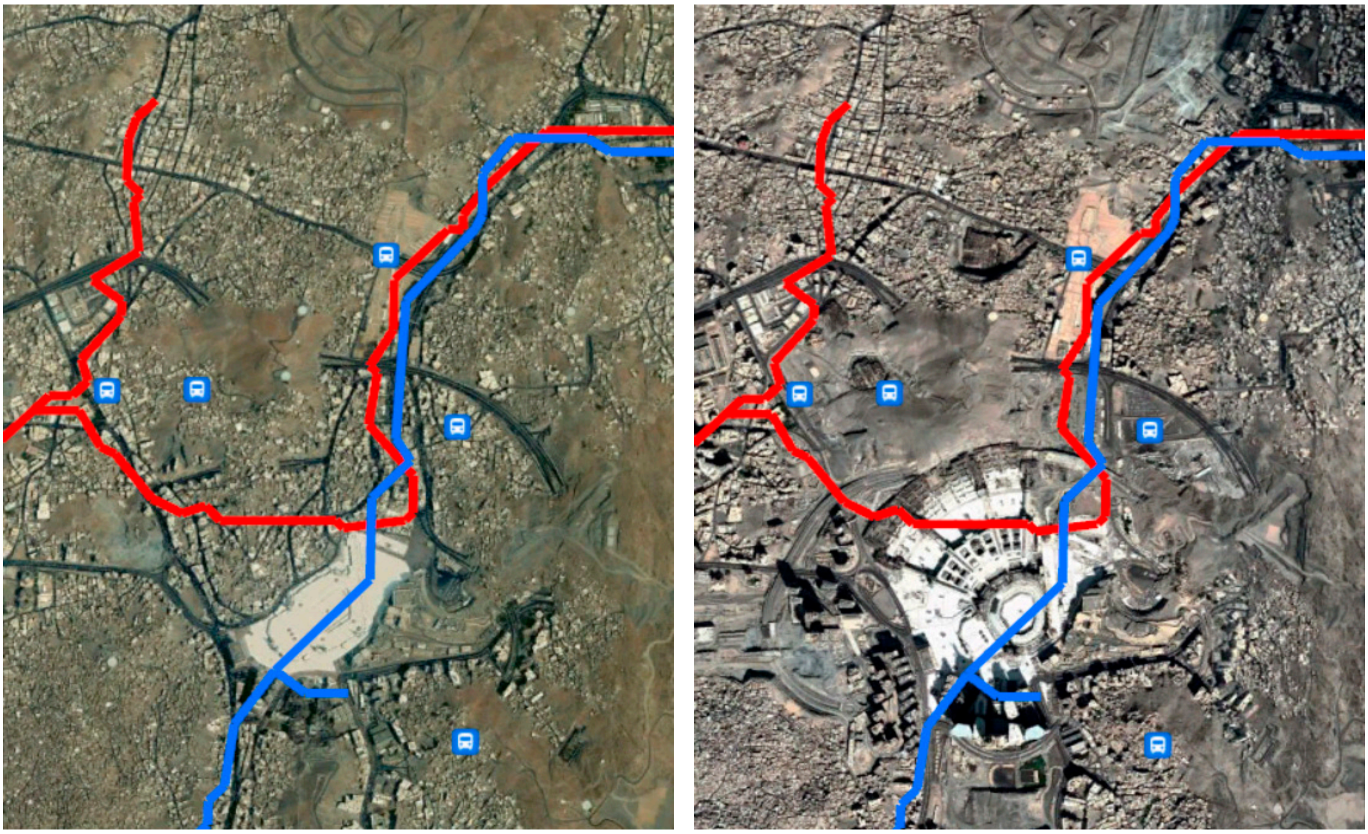

Figure 15. Stream network comparison based on historical imagery. Left in 2004 and right in 2021 (Google Earth).

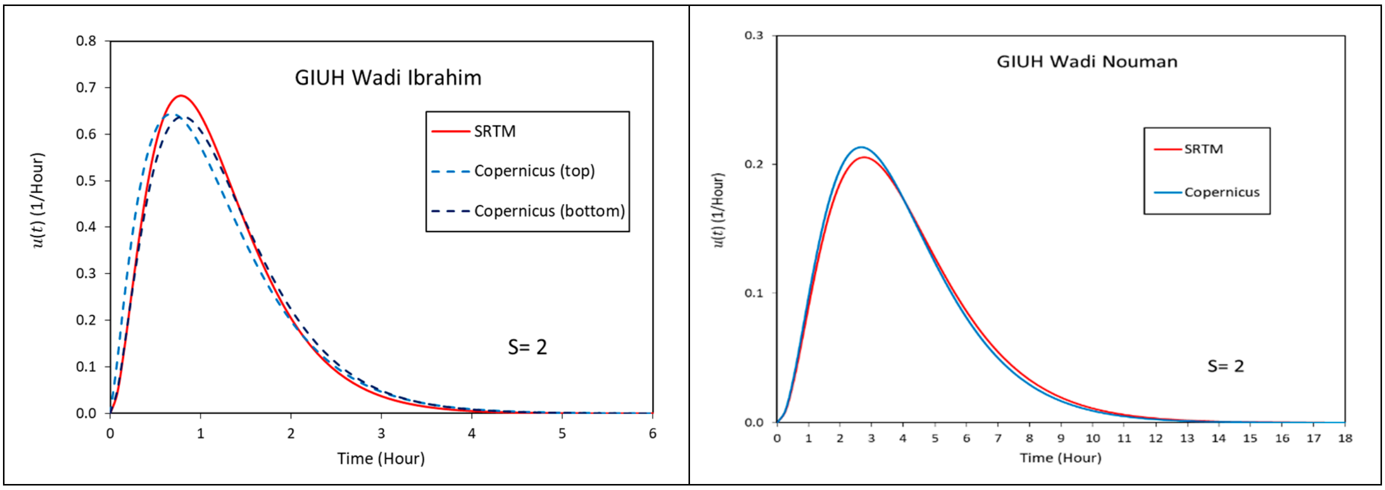

Figure 16. Comparison of GIUHs for SRTM vs. Copernicus.

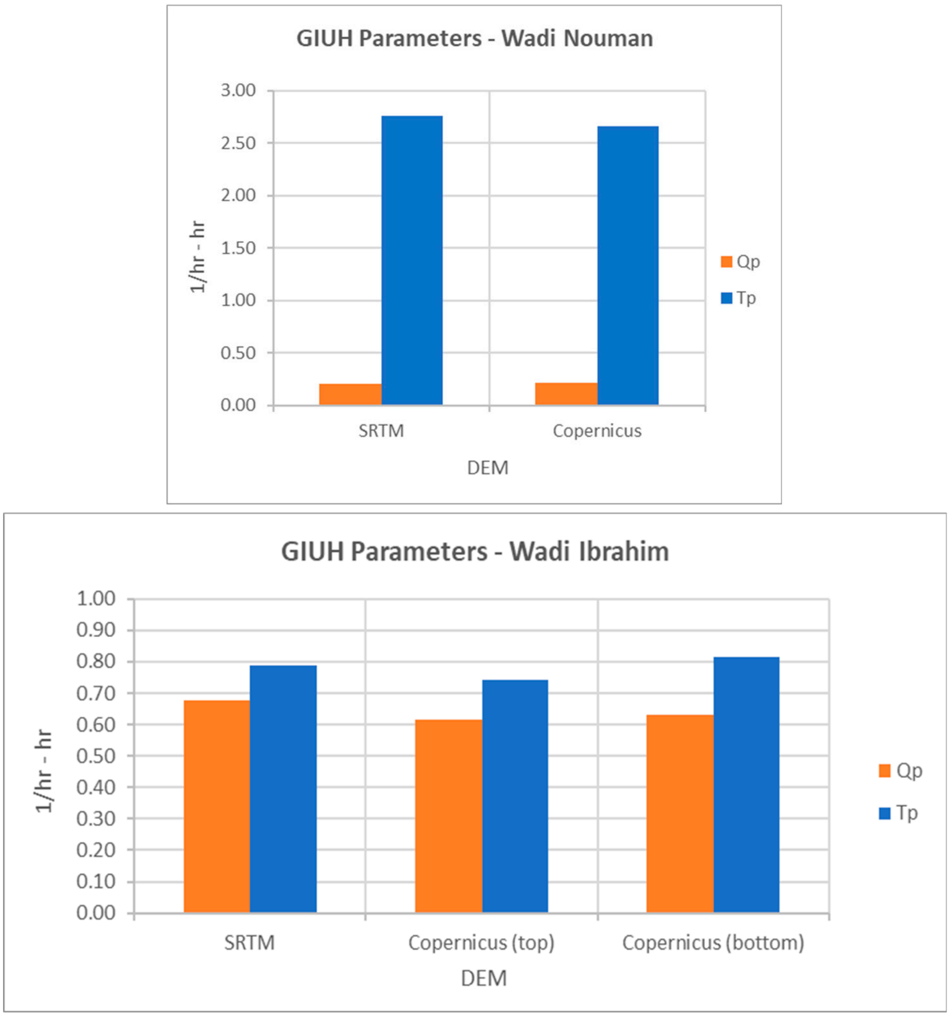

Figure 17. Variation of the GIUH parameters q_p and t_p for SRTM and Copernicus DEM.

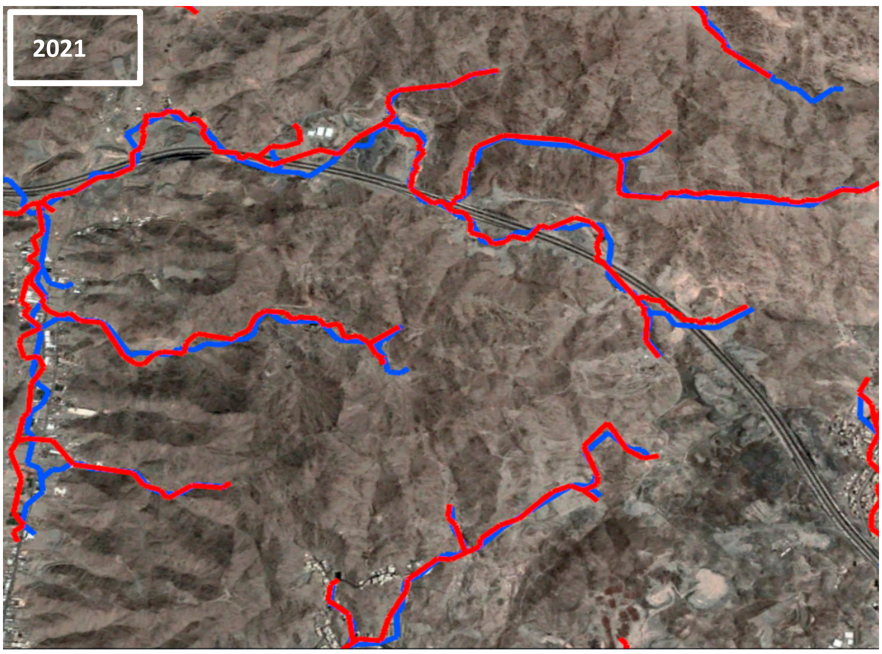

Figure 18. Stream network comparison in mountainous area (Google Earth).

Figure 13 shows the SRTM DEM; the blue line represents the stream of SRTM, and the red line represents the stream of Copernicus. The stream direction is straight in the south-western direction towards the outlet, while in the Copernicus images, the stream flow turns to the western direction due to the hill being removed (black oval mark), so the stream flow can reroute through that area.

Figure 14 shows a cross-section of two lines (A–A′ and B–B′). The elevation of the Copernicus has decreased from approximately 355 m to 307 m on AA′, and from 361 m to 302 m on BB′. Figure 15 strengthens the explanations of this phenomenon, where changes in the stream network occurred in the Haram Mosque area. Some hilly areas are being removed as part of the mega project's expansion of the Al-Haram Mosque. The Copernicus stream's direction does not go through the Haram Mosque area like SRTM, but moves to its surroundings following the pattern of the mosque as the recent terrain surface condition based on the year 2019 on Google Earth Pro. This makes sense and is more logical for Copernicus compared to the SRTM DEM.

To study the anthropogenic effects on hydrological responses, the GIUH and Hydrological stream network analysis was performed as well. Table 7 shows the Horton–Strahler ratio parameters (R_B, R_L and R_A) of Wadi Nouman and Wadi Ibrahim catchments. These data were obtained by plotting $N(w)$, $L(w)$, and $A(w)$ versus order w on a semi-log diagram.

Table 7. Horton–Strahler ratios of three wadies based on four DEM datasets.

Basin	DEM	Horton Ratios			
		R_L	R_B	R_A	L_Ω (m)
Wadi Nouman	SRTM	2.61	4.62	5.28	33,672
	Copernicus	2.58	4.8	5.44	31,740
Wadi Ibrahim	SRTM	1.55	2.74	3.27	5407
	Copernicus (top)	9.7	6	11.28	14,409
	Copernicus (bottom)	1.65	3.32	4.28	5939

The comparison of the GIUH hydrograph can be seen in Figure 16. Each GIUH has a different shape and q_p and t_p due to different of Horton–Strahler ratios, with a threshold area (S) of 2 km^2. The Figure 16 shows Copernicus has the highest q_p and lowest t_p compared to SRTM for Wadi Nouman, while in Wadi Ibrahim, SRTM has a higher q_p than Copernicus. The q_p and t_p parameters of the bottom catchment are higher than the top catchment. The summaries of the q_p and t_p comparison of all wadies is shown in Figure 17.

The shape of the GIUH depends on the Horton ratios, especially L_Ω. In wadi Nouman, the GIUH of SRTM and Copernicus look similar. Based on the significance test of 95% level of confidence and the one-tailed test, the difference between Wadi Nouman and Wadi Ibrahim is not significant. Wadi Nouman has a t-value 0.14536 and *p*-value of 0.442229; Wadi Ibrahim (bottom) has a t-value of −0.24954 and *p*-value of 0.4015; and Wadi Ibrahim (top) has a t-value of −0.40449 and *p*-value of 0.342974.

The last investigation is based on the location. The mountainous area (Figure 18) (Latitude 21°30′56.38″ N and longitude 39°50′22.11″ E) has a highly similar pattern for SRTM and Copernicus due to the dominant influence of the mountainous relief and relatively inconsequential influence of anthropogenic activities and DSM noise, while in the urban area (Figure 19) (Latitude 21°21′42.16″ N and longitude 39°49′45.46″ E), the variation of the stream network is high due to differing DSM noise and significant anthropogenic activities, such as urban redevelopment. The stream flow direction of Copernicus provides high accuracy by smoothly following the road as the stream network.

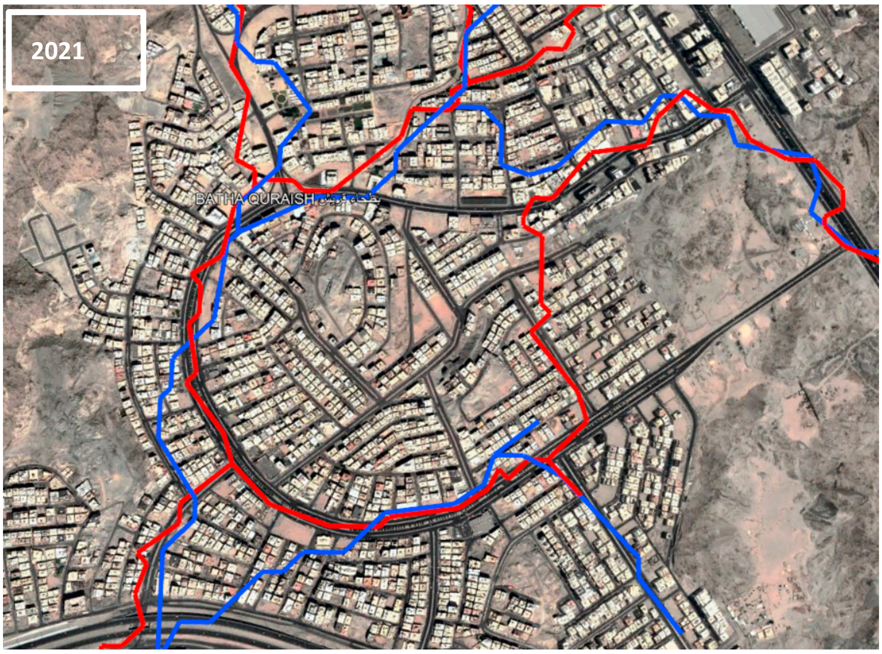

Figure 19. Stream network comparison in the urban or plain area (Google Earth).

5. Discussions

5.1. Limitation of Sentinel-1 DEM

In this study, the Sentinel-1 DEM was obtained using the InSAR technique. The limitation of the DEM InSAR technique depends on the data used and characteristics such as the microwave radar band [40,41]. Makkah City is a suitable area due to DEM InSAR having reliable results for no or fewer vegetation areas [34,41]. However, the DEM generation of Sentinel-1 is challenging, especially in selecting a suitable baseline. The small perpendicular baseline is sensitive to noise and atmospheric artifacts, which produce poor results; between 150 m and 300 m is the optimum baseline. The short temporal baseline should be as short as possible to reduce the risk of phase decorrelation. In this study, the selection process of data was carried out carefully. There are eight pairs of images with various perpendicular and temporal baselines ranging from 107 to 191 m and 12 days to 191 m, respectively. The coherence ranges from 0.83 to 0.89. The best results to come from the baseline are 153 m and 12 days. Unfortunately, the temporal baseline of 6 days is not available in Makkah City. A suitable perpendicular baseline, short temporal baseline, and good atmospheric conditions for data acquisition are essential to obtain good DEM results [34,42].

5.2. DEM, GIUH, and Stream Network Comparison

This study compared four DEM datasets: three DEM that are open global DEM and Sentinel-1 DEM, which have different band waves. The L-band, C-band, and X-band have different interactions with surface objects. Sentinel-1 DEM is generated manually from two Sentinel-1 images using the InSAR technique [34,43]. The assessment or validation DEM contains statistical measurements such as elevation error, MAE, RMSE, and R^2. The elevation error is based on the difference between the elevation of four DEM datasets to topographic maps as reference data. This measurement can represent vertical accuracy and be used in the previous study [44]. GIUH and stream network comparisons were applied to assess the accuracy of the DEMs. Copernicus has a robust performance, with the smallest elevation error and RMSE, and Sentinel-1 is the worst of all. These results can be caused by differences in the number of sample points, as well as different sources and data collection techniques.

In hydrological analysis, there are differences in R_B, R_L, R_A, L_Ω and the main length of the stream for all DEMs. These conditions make different GIUH shapes, which are generated based on the Nash model [38] and built based on Horton–Strahler ratio parameters. Based on the GIUH, there are changes in the shape of the q_p and t_p parameters for all DEMs and catchments. In the hydrology stream network comparison, the stream network in the mountainous area has quite a similar pattern [45], while having a notable difference in the urban area [46]. As mentioned in the study area, Makkah City has complex places in which mountains appear along the residential urban area. These conditions may have an impact on human modification and construction projects in Makkah City. Based on the base map on Google Earth Pro in 2021, Copernicus has more accuracy than SRTM, which follows the recent and up-to-date condition of the terrain surface of Makkah City. This result matches that of a previous study that the Copernicus DEM has the most realistic height representation and the highest quality landscape representation, is the preferred DEM for topographic analysis [23] and a more accurate representation of the earth's surface [47], is the optimum and most accurate DEM with regard to vertical accuracy, 1.3521 m and with 95% confidence level 2.6502 m [48], has the highest vertical accuracy of mean error, standard deviation, the lowest RMSE, and is most similar to the reference DEM [24].

6. Conclusions

The stream network changes in the catchment in Makkah City have been analyzed through DEM datasets. The assessment of various DEM datasets was performed to select the up-to-date DEM that represents current conditions, since no DEM is free from error, considering area condition, acquisition method, acquisition period, and characteristic of the band wave. Based on this study, the following conclusions can be obtained:

- Based on SAR data availability in Makkah City, the best results generated with lower errors compared to other pair images were obtained on 10 December and 22 December 2022. Despite having lower errors, the quality of the Sentinel-1 DEM needs to be improved by using images within a suitable perpendicular baseline, short temporal baseline, and good atmospheric conditions for data acquisition.
- Based on the DEM elevation comparison, Copernicus and SRTM have the highest accuracy, with R^2 = 0.9788 and 0.9765 and the lowest RMSE 3.89 m and 4.23 m, respectively. Sentinel-1 and ALOS have the lowest R^2 of 0.9028 and 0.9688, and the highest RMSE of 6.31 m and 4.27 m, respectively.
- In Wadi Ibrahim, it was found that the catchment is divided into two sub-wadis based on the Copernicus DEM. This main change in the drainage system in Wadi Ibrahim was due to the continuum of anthropogenic (human) activities around the holy city of Mecca (the mega project of the holy mosque expansion, demolishing mountains, adding buildings, etc.)
- The stream network and the morphometric parameters (Horton–Strahler ratios) of the catchments vary for both Copernicus and SRTM DEMs and influence the shape of the GIUH.
- The Copernicus DEM for Wadi Nouman has a higher q_p and lower t_p (0.21 and 2.66) than SRTM (0.20 and 2.75). In Wadi Ibrahim, the SRTM has a greater q_p and lower t_p than Copernicus due to the wadi being divided into two sub-wadies.
- The stream network in the mountainous area is quite similar for SRTM and Copernicus due to the dominant influence of the mountainous relief and relatively inconsequential influence of anthropogenic activities and DSM noise. In the urban area, the variation of the stream network is high due to differing DSM noise and significant anthropogenic activities such as urban redevelopment.
- Overall, the Copernicus DEM features the most reliable data quality compared to other open-source data and represents the most recent data.

Author Contributions: Conceptualization, M.E.; Data curation, A.H.; Formal analysis, A.H. and L.Z.; Funding acquisition, L.Z.; Investigation, L.Z.; Methodology, A.H. and A.C.; Validation, A.C.; Visualization, A.C.; Writing—original draft, M.E.; Writing—review & editing, M.E. All authors have read and agreed to the published version of the manuscript.

Funding: This project was funded by the Deanship of Scientific Research (DSR), King Abdulaziz University, Jeddah, under Grant No. (G-51-155-1442). The authors, therefore, acknowledge with thanks, DSR technical and financial support.

Data Availability Statement: Publicly available datasets were analyzed in this study.

Conflicts of Interest: The authors declare no conflict of interest.

References

1. Chandesris, A.; Van Looy, K.; Diamond, J.S.; Souchon, Y. Small dams alter thermal regimes of downstream water. *Hydrol. Earth Syst. Sci.* **2019**, *23*, 4509–4525. [CrossRef]
2. Elhag, M.; Galal, H.K.; Alsubaie, H. Understanding of morphometric features for adequate water resource management in arid environments. *Geosci. Instrum. Methods Data Syst.* **2017**, *6*, 293–300. [CrossRef]
3. Wang, W.; Shao, Q.; Yang, T.; Peng, S.; Xing, W.; Sun, F.; Luo, Y. Quantitative assessment of the impact of climate variability and human activities on runoff changes: A case study in four catchments of the Haihe River basin, China. *Hydrol. Process.* **2013**, *27*, 1158–1174. [CrossRef]
4. Tang, X.; Fu, G.; Zhang, S.; Gao, C.; Wang, G.; Bao, Z.; Jin, J. Attribution of climate change and human activities to streamflow variations with a posterior distribution of hydrological simulations. *Hydrol. Earth Syst. Sci. Discuss.* **2021**, *2021*, 1–37. [CrossRef]
5. Güler, C.; Kurt, M.A.; Alpaslan, M.; Akbulut, C. Assessment of the impact of anthropogenic activities on the groundwater hydrology and chemistry in Tarsus coastal plain (Mersin, SE Turkey) using fuzzy clustering, multivariate statistics and GIS techniques. *J. Hydrol.* **2012**, *414*, 435–451. [CrossRef]
6. Sadeghi, S.H.; Hazbavi, Z.; Gholamalifard, M. Interactive impacts of climatic, hydrologic and anthropogenic activities on watershed health. *Sci. Total Environ.* **2019**, *648*, 880–893. [CrossRef] [PubMed]
7. Bao, Z.; Zhang, J.; Wang, G.; Fu, G.; He, R.; Yan, X.; Jin, J.; Liu, Y.; Zhang, A. Attribution for decreasing streamflow of the Haihe River basin, northern China: Climate variability or human activities? *J. Hydrol.* **2012**, *460*, 117–129. [CrossRef]
8. Kong, D.; Miao, C.; Wu, J.; Duan, Q. Impact assessment of climate change and human activities on net runoff in the Yellow River Basin from 1951 to 2012. *Ecol. Eng.* **2016**, *91*, 566–573. [CrossRef]
9. Han, Z.; Long, D.; Fang, Y.; Hou, A.; Hong, Y. Impacts of climate change and human activities on the flow regime of the dammed Lancang River in Southwest China. *J. Hydrol.* **2019**, *570*, 96–105. [CrossRef]
10. Xie, J.; Xu, Y.-P.; Wang, Y.; Gu, H.; Wang, F.; Pan, S. Influences of climatic variability and human activities on terrestrial water storage variations across the Yellow River basin in the recent decade. *J. Hydrol.* **2019**, *579*, 124218. [CrossRef]
11. Kumar, A.U.; Jayakumar, K. Hydrological alterations due to anthropogenic activities in Krishna River Basin, India. *Ecol. Indic.* **2020**, *108*, 105663. [CrossRef]
12. Yang, N.; Zhang, Y.; Duan, K. Effect of hydrologic alteration on the community succession of macrophytes at Xiangyang Site, Hanjiang River, China. *Scientifica* **2017**, *2017*, 4083696. [CrossRef] [PubMed]
13. Zhang, Y.; Arthington, A.; Bunn, S.; Mackay, S.; Xia, J.; Kennard, M. Classification of flow regimes for environmental flow assessment in regulated rivers: The Huai River Basin, China. *River Res. Appl.* **2012**, *28*, 989–1005. [CrossRef]
14. Jing, C.; Shortridge, A.; Lin, S.; Wu, J. Comparison and validation of SRTM and ASTER GDEM for a subtropical landscape in Southeastern China. *Int. J. Digit. Earth* **2014**, *7*, 969–992. [CrossRef]
15. Jenson, S.K.; Domingue, J.O. Extracting topographic structure from digital elevation data for geographic information system analysis. *Photogramm. Eng. Remote Sens.* **1988**, *54*, 1593–1600.
16. Farran, M.M.; Elfeki, A.; Elhag, M.; Chaabani, A. A comparative study of the estimation methods for NRCS curve number of natural arid basins and the impact on flash flood predications. *Arab. J. Geosci.* **2021**, *14*, 1–23. [CrossRef]
17. Tarboton, D.G. A new method for the determination of flow directions and upslope areas in grid digital elevation models. *Water Resour. Res.* **1997**, *33*, 309–319. [CrossRef]
18. Elhag, M.; Yilmaz, N. Insights of remote sensing data to surmount rainfall/runoff data limitations of the downstream catchment of Pineios River, Greece. *Environ. Earth Sci.* **2021**, *80*, 1–13. [CrossRef]
19. Erskine, R.H.; Green, T.R.; Ramirez, J.A.; MacDonald, L.H. Comparison of grid-based algorithms for computing upslope contributing area. *Water Resour. Res.* **2006**, *42*, W09416. [CrossRef]
20. Boreggio, M.; Bernard, M.; Gregoretti, C. Evaluating the differences of gridding techniques for Digital Elevation Models generation and their influence on the modeling of stony debris flows routing: A case study from Rovina di Cancia basin (North-eastern Italian Alps). *Front. Earth Sci.* **2018**, *6*, 89. [CrossRef]
21. Hawker, L.; Bates, P.; Neal, J.; Rougier, J. Perspectives on digital elevation model (DEM) simulation for flood modeling in the absence of a high-accuracy open access global DEM. *Front. Earth Sci.* **2018**, *6*, 233. [CrossRef]

22. Saksena, S.; Merwade, V. Incorporating the effect of DEM resolution and accuracy for improved flood inundation mapping. *J. Hydrol.* **2015**, *530*, 180–194. [CrossRef]
23. Purinton, B.; Bookhagen, B. Beyond Vertical Point Accuracy: Assessing Inter-pixel Consistency in 30 m Global DEMs for the Arid Central Andes. *Front. Earth Sci.* **2021**, *9*, 758606. [CrossRef]
24. Karlson, M.; Bastviken, D.; Reese, H. Error Characteristics of Pan-Arctic Digital Elevation Models and Elevation Derivatives in Northern Sweden. *Remote Sens.* **2021**, *13*, 4653. [CrossRef]
25. Karki, S.; Acharya, S.; Gautam, A. Evaluation of the Vertical Accuracy of Open Access Digital Elevation Models across Different Physiographic Regions and 2 River Basins of Nepal 3. 2021. Available online: https://www.researchgate.net/profile/Saroj-Karki-5/publication/351927834_Evaluation_of_the_Vertical_Accuracy_of_Open_Access_Digital_Elevation_Models_across_Different_Physiographic_Regions_and_River_Basins_of_Nepal/links/60b51a2092851cde8846dad9/Evaluation-of-the-Vertical-Accuracy-of-Open-Access-Digital-Elevation-Models-across-Different-Physiographic-Regions-and-River-Basins-of-Nepal.pdf (accessed on 17 July 2022).
26. Masoud, M.H.; Basahi, J.; Niyazi, B. Assessment and modeling of runoff in ungauged basins based on paleo-flood and GIS techniques (case study of Wadi Al Dawasir-Saudi Arabia). *Arab. J. Geosci.* **2019**, *12*, 483. [CrossRef]
27. Bahrawi, J.; Alqarawy, A.; Chabaani, A.; Elfeki, A.; Elhag, M. Spatiotemporal analysis of the annual rainfall in the Kingdom of Saudi Arabia: Predictions to 2030 with different confidence levels. *Theor. Appl. Climatol.* **2021**, *146*, 1479–1499. [CrossRef]
28. Rodríguez-Iturbe, I.; Valdés, J.B. The geomorphologic structure of hydrologic response. *Water Resour. Res.* **1979**, *15*, 1409–1420. [CrossRef]
29. Moussa, R. Definition of new equivalent indices of Horton-Strahler ratios for the derivation of the Geomorphological Instantaneous Unit Hydrograph. *Water Resour. Res.* **2009**, *45*, W09406. [CrossRef]
30. Shaaban, F.; Othman, A.; Habeebullah, T.M.; El-Saoud, W.A. An integrated GPR and geoinformatics approach for assessing potential risks of flash floods on high-voltage towers, Makkah, Saudi Arabia. *Environ. Earth Sci.* **2021**, *80*, 199. [CrossRef]
31. Elhag, M.; Alshamsi, D. Integration of remote sensing and geographic information systems for geological fault detection on the island of Crete, Greece. *Geosci. Instrum. Methods Data Syst.* **2019**, *8*, 45–54. [CrossRef]
32. El Bastawesy, M.; Al Harbi, K.; Habeebullah, T. The hydrology of Wadi Ibrahim Catchment in Makkah City, the Kingdom of Saudi Arabia: The interplay of urban development and flash flood hazards. *Life Sci. J.* **2012**, *9*, 580–589.
33. Yousef, B. The climate of Mecca area. *J. Umm Al-Qura Soc. Sci.* **1992**, *15*, 1–94.
34. Braun, A. Retrieval of digital elevation models from Sentinel-1 radar data–open applications, techniques, and limitations. *Open Geosci.* **2021**, *13*, 532–569. [CrossRef]
35. Sahoo, R.; Jain, V. Sensitivity of drainage morphometry based hydrological response (GIUH) of a river basin to the spatial resolution of DEM data. *Comput. Geosci.* **2018**, *111*, 78–86. [CrossRef]
36. Bamufleh, S.; Al-Wagdany, A.; Elfeki, A.; Chaabani, A. Developing a geomorphological instantaneous unit hydrograph (GIUH) using equivalent Horton-Strahler ratios for flash flood predictions in arid regions. *Geomat. Nat. Hazards Risk* **2020**, *11*, 1697–1723. [CrossRef]
37. Horton, R.E. Erosional development of streams and their drainage basins; hydrophysical approach to quantitative morphology. *Geol. Soc. Am. Bull.* **1945**, *56*, 275–370. [CrossRef]
38. Nash, J.E.; HRS. A unit hydrograph study, with particular reference to British catchments. *Proc. Inst. Civ. Eng.* **1960**, *17*, 249–282. [CrossRef]
39. Rosso, R. Nash model relation to Horton order ratios. *Water Resour. Res.* **1984**, *20*, 914–920. [CrossRef]
40. Stilla, U.; Soergel, U.; Thoennessen, U. Potential and limits of InSAR data for building reconstruction in built-up areas. *ISPRS J. Photogramm. Remote Sens.* **2003**, *58*, 113–123. [CrossRef]
41. Castellazzi, P.; Arroyo-Domínguez, N.; Martel, R.; Calderhead, A.I.; Normand, J.C.; Gárfias, J.; Rivera, A. Land subsidence in major cities of Central Mexico: Interpreting InSAR-derived land subsidence mapping with hydrogeological data. *Int. J. Appl. Earth Obs. Geoinf.* **2016**, *47*, 102–111. [CrossRef]
42. Hanssen, R.F. *Radar Interferometry: Data Interpretation and Error Analysis*; Springer: Berlin/Heidelberg, Germany, 2001; Volume 2.
43. Elhag, M.; Bahrawi, J.; Aljahdali, M.H.; Eleftheriou, G.; Labban, A.H.; Alqarawy, A. Vertical displacement assessment in temporal analysis of the transboundary islands of Tiran and Sanafir, Egypt-Saudi Arabia. *Arab. J. Geosci.* **2022**, *15*, 1–13. [CrossRef]
44. del Rosario Gonzalez-Moradas, M.; Viveen, W. Evaluation of ASTER GDEM2, SRTMv3. 0, ALOS AW3D30 and TanDEM-X DEMs for the Peruvian Andes against highly accurate GNSS ground control points and geomorphological-hydrological metrics. *Remote Sens. Environ.* **2020**, *237*, 111509. [CrossRef]
45. Elhag, M.; Hidayatulloh, A.; Bahrawi, J.; Chaabani, A.; Budiman, J. Using inconsistencies of wadi morphometric parameters to understand patterns of soil erosion. *Arab. J. Geosci.* **2022**, *15*, 1–14. [CrossRef]
46. Bahrawi, J.; Ewea, H.; Kamis, A.; Elhag, M. Potential flood risk due to urbanization expansion in arid environments, Saudi Arabia. *Nat. Hazards* **2020**, *104*, 795–809. [CrossRef]
47. Marešová, J.; Gdulová, K.; Pracná, P.; Moravec, D.; Gábor, L.; Prošek, J.; Barták, V.; Moudrý, V. Applicability of Data Acquisition Characteristics to the Identification of Local Artefacts in Global Digital Elevation Models: Comparison of the Copernicus and TanDEM-X DEMs. *Remote Sens.* **2021**, *13*, 3931. [CrossRef]
48. Mutar, A.Q.; Mustafa, M.T.; Hameed, M.A. The impact of (DEM) Accuracy on the Watersheds areas as a function of spatial data. *Period. Eng. Nat. Sci.* **2021**, *9*, 1118–1130. [CrossRef]